Ultrafast Pump–Probe Spectroscopy: Femtosecond Dynamics in Liouville Space

Yi Jing Yan, Laurence E. Fried,[†] and Shaul Mukamel[*,‡]

Chemistry Department, University of Rochester, Rochester, New York 14627 (Received: May 23, 1989)

A theory for ultrafast pump–probe spectroscopy is developed using a correlation function description of molecular nonlinear optical processes which is based on the density matrix and its evolution in Liouville space. The Liouville space description applies to isolated small molecules as well as complex systems in condensed phases. We identify a condition, called *ultrafast dephasing*, which allows the probe absorption to be written in terms of an intuitive picture of instantaneous preparation, field-free evolution, and instantaneous detection. The probe absorption is calculated by following a phase-space *doorway function* which is prepared by the pump, propagates for a specified delay, and is finally projected into a *window function* which depends on the probe frequency. We find that the doorway and window functions have well-known classical limits: the delta functions in coordinate appearing in the classical Condon approximation. The deviation of the doorway and window functions from their classical limits is a direct and visual measure of the importance of quantum corrections in pump–probe spectroscopy. The signal consists of a sequential term and a tunneling (coherent) term which are formally analogous to fluorescence and Raman line shapes, respectively. Application is made to the femtosecond photodissociation of ICN, where the importance of quantum corrections and the tunneling term is assessed. The role of dephasing processes and the relation to other spectroscopic techniques related to the nonlinear susceptibility $\chi^{(3)}$ are discussed.

I. Introduction

Recent experimental progress in laser spectroscopy, in particular the development of ultrafast tunable lasers, has made it possible to conduct nonlinear optical measurements using carefully timed and tuned multiple laser pulses. These techniques allow femtosecond dynamical processes to be directly probed.[1-11]

The simplest multiple-pulse laser technique is pump–probe spectroscopy, in which the system is excited with a pump pulse and the absorption of a second probe pulse is measured as a function of the pump frequency, the probe frequency, and their relative delay. Femtosecond pump–probe techniques have been applied successfully to the study of the photophysics of dye molecules, primary biological processes, the solvated electron, and excitons and electron–hole pairs in semiconductors. Most recently Rosker, Dantus, and Zewail[12] succeeded in carrying out the first two-color femtosecond pump–probe experiment in a supersonic beam. In that experiment the photodissociation of ICN was directly monitored, allowing for the first time the observation of a bond breaking. This possibility of observing elementary chemical events in real time constitutes a fundamental breakthrough in the understanding of molecular dynamics. Bersohn and Zewail[12c] have offered a simple semiclassical interpretation of the ICN experiment using the classical Franck–Condon principle. It should be noted that pump–probe spectroscopy is one member of a broad class of nonlinear optical techniques[13-15] related to the *third-order optical polarization* $P^{(3)}$ and the corresponding *susceptibility* $\chi^{(3)}$. There are numerous such techniques which differ by the nature of the pulse sequence, the geometry and the choice of a spatial direction (phase matching), and the mode of detection. Some common techniques are four-wave mixing, time-resolved CARS (coherent anti-Stokes Raman), photon echoes and hole burning, transient grating, and stimulated pumping.[16-21]

In the present paper, we develop a new description of ultrafast pump–probe spectroscopy based on its $P^{(3)}$ character and apply it to the ICN photodissociation. Our description provides a connection with a host of related nonlinear spectroscopies. The systematic methodology for the analysis and the interpretation of molecular nonlinear optical measurements is based on the density matrix formulation of quantum mechanics (known as Liouville space).[15] We emphasize that the more narrow goal of calculating the results of the ICN experiment can be readily accomplished without the use of the present Liouville space machinery. Although calculations are reported here, our goal is not the development of efficient numerical techniques applicable to

ICN photodissociation at zero temperature. Rather, we present a novel picture of the ICN photodissociation based on a quantum phase-space (Wigner function) representation of the density matrix.[22] The semiclassical picture suggested by Bersohn and

(1) See papers in: *Ultrafast Phenomena VI*; Yajima, T., Yoshihara, K., Harris, C. B., Shionoya, S., Eds.; Springer-Verlag: Berlin, 1988.

(2) Fleming, G. R. *Chemical Applications of Ultrafast Spectroscopy*; Oxford University Press: London, 1986.

(3) Brito Cruz, C. H.; Fork, R. L.; Knox, W.; Shank, C. V. *Chem. Phys. Lett.* **1986**, *132*, 341. Becker, P. C.; Fork, R. L.; Brito Cruz, C. H.; Gordon, J. P.; Shank, C. V. *Phys. Rev. Lett.* **1988**, *60*, 2462. Becker, P. C.; Fragnito, H. L.; Bigot, J. Y.; Brito Cruz, C. H.; Fork, R. L.; Shank, C. V. *Phys. Rev. Lett.* **1989**, *63*, 505.

(4) (a) Migus, A.; Gauduel, Y.; Martin, J. L.; Antonetti, A. *Phys. Rev. Lett.* **1987**, *58*, 1559. (b) Oudar, J. L.; Hulin, D.; Migus, A.; Antonetti, A.; Alexandre, F. *Phys. Rev. Lett.* **1985**, *55*, 2074. Peyghambarian, N.; Koch, S. W. *Rev. Phys. Appl.* **1987**, *22*, 61.

(5) Knox, W. H.; Chemla, D. S.; Miller, D. A. B.; Stark, J. B.; Schmitt-Rink, S. *Phys. Rev. Lett.* **1989**, *62*, 1189. Peyghambarian, N.; Koch, S. W.; Lindberg, M.; Fluegel, B.; Joffre, M. *Phys. Rev. Lett.* **1989**, *62*, 1185.

(6) Yan, Y.; Cheng, L.; Nelson, K. A. *Advances in Nonlinear Spectroscopy*; Clark, R. J. H., Hester, R. E., Eds.; Wiley: New York, 1988. Yan, Y.; Nelson, K. A. *J. Chem. Phys.* **1987**, *87*, 6240, 6257.

(7) Rosker, M. J.; Wise, F. W.; Tang, C. L. *Phys. Rev. Lett.* **1986**, *57*, 321. Walmsley, I. A.; Mitsunaga, M.; Tang, C. L. *Phys. Rev. A* **1988**, *38*, 4681. Wise, F. W.; Rosker, M. J.; Tang, C. L. *J. Chem. Phys.* **1987**, *86*, 2827.

(8) Wiener, A. M.; DeSilvestri, S.; Ippen, E. W. *J. Opt. Soc. Am. B* **1985**, *2*, 654. Wiener, A. M.; Heritage, J. P.; Salehi, J. A. *Opt. Lett.* **1988**, *13*. Warren, W. S. *Science*, in press.

(9) McMorrow, D.; Lotshaw, W. T.; Kenney-Wallace, G. A. *IEEE J. Quantum Electron.* **1988**, *QE-24*, 443. McMorrow, D.; Lotshaw, W. T.; Dickson, T. R.; Kenney-Wallace, G. A. In Ref 1, p 545.

(10) Wiersma, D. A.; Duppen, K. *Science* **1987**, *237*, 1147.

(11) Chesnoy, J.; Mokhtari, A. *Phys. Rev. A* **1988**, *38*, 3566.

(12) (a) Zewail, A. H.; Bernstein, R. B. *Chem. Eng. News* **1988**, *66*, 24. (b) Rosker, M. J.; Dantus, M.; Zewail, A. H. *Science* **1988**, *241*, 1200. (c) Bersohn, R.; Zewail, A. H. *Ber. Bunsen. Phys. Chem.* **1988**, *92*, 373. (d) Dantus, M.; Rosker, M. J.; Zewail, A. H. *J. Chem. Phys.* **1988**, *89*, 6113, 6128.

(13) Bloembergen, N. *Nonlinear Optics*; Benjamin: New York, 1965. Shen, Y. R. *The Principles of Nonlinear Optics*; Wiley: New York, 1984.

(14) (a) Mukamel, S. *Phys. Rev. A* **1983**, *28*, 3480. (b) Boyd, R. W.; Mukamel, S. *Phys. Rev. A* **1984**, *29*, 1973.

(15) (a) Mukamel, S. *Phys. Rep.* **1982**, *93*, 1. (b) Mukamel, S. *Adv. Chem. Phys.* **1988**, *70*, 165. (c) Mukamel, S.; Loring, R. F. *J. Opt. Soc. Am. B* **1986**, *3*, 595.

(16) Laubereau, A.; Kaiser, W. *Rev. Mod. Phys.* **1978**, *50*, 607. Zinth, W.; Polland, H. J.; Laubereau, A.; Kaiser, W. *Appl. Phys. B* **1981**, *26*, 77.

(17) Jankowiak, R.; Small, G. J. *Science* **1987**, *237*, 618.

(18) Berg, M.; Walsh, C. A.; Narasimhare, L. R.; Littau, K. A.; Fayer, M. D. *J. Chem. Phys.* **1988**, *88*, 1564.

(19) Alivisatos, A. P.; Harris, A. L.; Levinos, N. J.; Steigerwald, M. L.; Brus, L. E. *J. Chem. Phys.* **1988**, *89*, 4001.

(20) Saiken, S. *Phys. Rev. A* **1988**, *38*, 4669. Saikan, S.; Nakabayashi, T.; Kanematsu, Y.; Tato, N. *Phys. Rev. B* **1988**, *38*, 7777; Genberg, L.; Heisel, F.; McLendon, G.; Dwayne Miller, R. J. *J. Phys. Chem.* **1987**, *91*, 5521. Fleming, G. R.; Martin, J. L.; Breton, J. *Nature* **1988**, *333*, 190.

(21) Bernstein, R. B.; Zewail, A. H. *J. Chem. Phys.* **1989**, *90*, 829.

Zewail[12c] appears more naturally within our framework than in a treatment based on wave functions. Our theory allows the importance of quantum corrections to pump-probe photodissociation to be directly visualized. This is a question of some interest, since the potential energy inversion technique proposed by Bersohn, Bernstein, and Zewail[12c,21] is based on classical mechanics. We relate the widths in coordinate of certain Wigner functions (called doorway and window functions) to the importance of quantum corrections in pump-probe spectroscopy; a wide doorway or window function implies that quantum corrections are significant.

The present treatment also corresponds closely to the way that pump-probe photodissociation is commonly thought of: a state (called a doorway function) is instantaneously prepared by the pump laser, which then evolves in the absence of the field on the dissociative electronic surface. Next, the evolving state is instantaneously probed by a second laser. We introduce a quantity, called the "bare spectrum", which corresponds to this process with a definite delay time between the pump and probe steps. The observed spectrum is a temporal convolution of the bare spectrum with the combined intensity profile of the pump and probe lasers. Wave function based treatments of femtosecond photodissociation cannot be expressed in terms of this simple language of preparation, evolution, and detection.

Another question of physical interest is the importance of time ordering of the pump and probe fields in the pump-probe signal. Clearly, if the pulse delay is much longer than the combined pump-probe temporal width, processes where the pump acts first and the probe acts second will dominate. For time delays comparable to the pump-probe temporal width, reversed time ordering where the *probe* may act before the *pump* can be important.[14] In instances where reversed processes are significant, care must be taken in interpreting the experimental signal. For instance, classical inversion procedures certainly cannot be used in this regime. An advantage of the density matrix formalism employed here is that we can separate ordinary and reversed terms in the *signal*. This is not possible with wave functions, since a wave function where the pump and probe pulses have a definite time ordering yields a signal that is not time-ordered. Also, our treatment allows femtosecond photodissociation experiments to be visualized at finite temperature and in condensed phases. The application to condensed phases, and in particular the development of a reduced description of optical processes whereby bath degrees of freedom are traced out, can only be made by using the density matrix. In particular, the concept of dephasing, which is a cornerstone in condensed-phase spectroscopy, shows up naturally in the present formulation. We can also make a connection to the dynamics of rate processes such as electron transfer.[23]

In summary, the advantages that we gain in a density matrix formalism are (1) a close relation to the common treatments of other nonlinear spectroscopies, (2) direct and visual insight into the importance of quantum corrections in the spectroscopy, (3) a simple physical picture of preparation, evolution, and detection, (4) the ability to directly ascertain the importance of reversed time orderings of the pump and probe field, and (5) a theory general enough to be used for finite-temperature processes in condensed phases. A Brownian oscillator model for vibrational and solvation dynamics was developed by using the Liouville space response function.[24] This model can be easily incorporated in the present theory. We believe that these benefits more than justify the added formal complexity entailed in a Liouville space description. This is not to say that wave function based treatments have no value or cannot be interpreted. There are, however, unique advantages entailed in a density matrix approach, and it is those advantages that we pursue here.

The rest of this paper is organized as follows: In section II we present the nonlinear response function related to the nonlinear

polarization $P^{(3)}$ with its eight Liouville space pathways. In section III we define the probe absorption in a pump-probe measurement. In section IV we show how the Liouville space description leads to the doorway/window picture which most closely resembles the semiclassical description of Bersohn and Zewail. In section V we present numerical calculations of the ICN spectrum. In section VI we give a detailed discussion and comparison of the Liouville space with the more common wave function description. Conclusions and a summary of our results are given in section VII.

II. Eight Pathways for the Nonlinear Response Function

In this section we review the density matrix approach to nonlinear spectroscopies. The third-order optical polarization $P^{(3)}$ is expressed in terms of a triple Fourier transform of a nonlinear response function,[13-15,25] which contains the complete microscopic information necessary for the interpretation of these experiments. The response function is expressed in an eigenstate-free form which allows it to be calculated directly in Liouville space.

Consider a nonlinear spectroscopic experiment in which the molecular system interacts with an external electric field $E(\mathbf{r},t)$. This field consists, in general, of a sequence of several incoming pulses. The various nonlinear optical spectroscopies mentioned in the Introduction differ by the timing, the detuning, and the direction of these pulses. The total Hamiltonian is

$$H_T = H + H_{int} \qquad (2.1)$$

where H is the material Hamiltonian in the absence of the external field. H_{int} represents the material-field interaction. In the electric dipole approximation we have

$$H_{int} = -VE(\mathbf{r},t) \qquad (2.2)$$

where V is the molecular dipole operator. In the following treatment we ignore the polarization of the electric field and the vector nature of the dipole operator V, since these properties are not essential in understanding pump-probe photodissociation spectroscopy. The optical properties of the system may be related to the time-dependent polarization

$$P(\mathbf{r},t) = \text{Tr}\ (V\rho(t)) \qquad (2.3)$$

Here $\rho(t)$ is the density matrix of the system, which satisfies the Liouville equation

$$d\rho/dt = -i[H,\rho] - i[H_{int},\rho] \equiv -i(L + L_{int})\rho \qquad (2.4)$$

The Liouville operators L and L_{int} defined in eq 2.4 are the commutators with H and H_{int}, respectively.

It is our aim to solve for $\rho(t)$ and thus the polarization $P(\mathbf{r},t)$ in a power series in H_{int}. The manipulations involved are most clearly and compactly expressed by using the Liouville space representation of quantum mechanics.[15,26] The main idea of the Liouville formulation is that *operators* form a Hilbert space in precisely the same way that *states* form a Hilbert space in more conventional formulations of quantum mechanics. A Liouville space operator maps a vector (ordinary operator) into another vector. For subsequent manipulations we shall introduce $\mathcal{V}$, the Liouville space dipole operator, by its action on an arbitrary operator A, $\mathcal{V}A \equiv [V,A]$.

The polarization $P(\mathbf{r},t)$ can be expanded in powers of E by solving the Liouville equation (eq 2.4) perturbatively in L_{int}. We get[13]

$$P(\mathbf{r},t) = \sum_{n=1}^{\infty} P^{(n)}(\mathbf{r},t) \qquad (2.5)$$

Each order in this expansion represents a different class of optical measurements. The linear polarization $P^{(1)}$ is responsible for linear optics, $P^{(2)}$ represents second-order nonlinear processes such as frequency sum generation, and $P^{(3)}$ is the third-order polarization which represents a broad variety of four-wave mixing spectroscopies. The corresponding susceptibilities are denoted $\chi^{(1)}$, $\chi^{(2)}$,

(22) Hillery, M.; O'Connel, R. F.; Scully, M. O.; Wigner, E. P. *Phys. Rep.* **1984**, *106*, 121.

(23) (a) Mukamel, S.; Yan, Y. J. *Acc. Chem. Res.* **1989**, *22*, 301. (b) Hu, Y.; Mukamel, S. *Chem. Phys. Lett.* **1989**, *160*, 410.

(24) Yan, Y. J.; Mukamel, S. *J. Chem. Phys.* **1988**, *88*, 5735; **1988**, *89*, 5160.

(25) Butcher, P. N. *Nonlinear Optical Phenomena*; Ohio University Press: Athens, OH, 1965.

(26) Fano, U. *Phys. Rev.* **1963**, *131*, 259. Ben Reuven, A. *Adv. Chem. Phys.* **1975**, *33*, 235.

and $\chi^{(3)}$, respectively. It has been shown[14] that pump–probe spectroscopy is obtained from $P^{(3)}$. A straightforward expansion of the Liouville equation yields[15b,c,24,27]

$$P^{(3)}(\mathbf{r},t) = \int_0^\infty dt_1 \int_0^\infty dt_2 \int_0^\infty dt_3 \, S^{(3)}(t_3,t_2,t_1) \, E(\mathbf{r},t-t_3) \times$$
$$E(\mathbf{r},t-t_3-t_2) \, E(\mathbf{r},t-t_3-t_2-t_1) \quad (2.6)$$

Here $S^{(3)}(t_3,t_2,t_1)$ is the third-order *nonlinear response function*

$$S^{(3)}(t_3,t_2,t_1) = -i \, \mathrm{Tr} \, \{ V\mathcal{G}(t_3) \, \mathcal{V}\mathcal{G}(t_2) \, \mathcal{V}\mathcal{G}(t_1) \, \mathcal{V}\rho(-\infty) \} \quad (2.7)$$

$\mathcal{G}(\tau)$ is the time evolution operator (Green function) of the Liouville equation in the absence of the external field, defined by its action on an arbitrary dynamical variable A

$$\mathcal{G}(t)A \equiv \exp(-iLt)A = \exp(-iHt)A \exp(iHt) \quad (2.8)$$

$S^{(3)}$ is the key quantity in the present article. It contains the complete microscopic information necessary for the calculation of any $P^{(3)}$ measurement, such as pump–probe spectroscopy. Physically, $S^{(3)}$ gives the polarization response to three δ function laser pulses. The time arguments t_1, t_2, and t_3 represent the time intervals between successive interactions with the electric field.

Let us consider the calculation of $S^{(3)}$ in eq 2.7. We start with the system in thermal equilibrium with density matrix $\rho(-\infty)$. We then act with the first $\mathcal{V}$, propagate freely for a period t_1, act with the second $\mathcal{V}$, propagate freely for a period t_2, act with the third $\mathcal{V}$, and propagate freely for a period t_3. Finally, we act with V from the left and take a trace. In order to treat the propagations in t_1, t_2, and t_3 explicitly, we introduce a molecular model relevant to the pump–probe experiment. We assume that the molecular system has three electronic states, denoted $|g\rangle$ (the ground state), $|e\rangle$ (an intermediate electronic state), and $|f\rangle$ (the final excited electronic state). The molecular Hamiltonian is given by

$$H = |g\rangle H_g \langle g| + |e\rangle H_e \langle e| + |f\rangle H_f \langle f| \quad (2.9)$$

and the dipole operator is

$$V = \mu_{ge}(\mathbf{Q})|g\rangle\langle e| + \mu_{eg}(\mathbf{Q})|e\rangle\langle g| + \mu_{ef}(\mathbf{Q})|e\rangle\langle f| + \mu_{fe}(\mathbf{Q})|f\rangle\langle e| \quad (2.10)$$

The adiabatic Hamiltonian H_ν (ν = g, e, or f) in eq 2.9 describes the nuclear degrees of freedom $\mathbf{Q}$ of the molecule in its electronic state $|\nu\rangle$. We further assume that the molecule is initially at thermal equilibrium in the vibronic manifold belonging to electronic level $|g\rangle$, with the density matrix $\rho(-\infty) = |g\rangle\rho_g\langle g|$.

In practice, the time evolution of coupled electronic and nuclear degrees of freedom required in eq 2.7 is difficult to solve without additional simplifications. Such simplifications can be made, however, if we keep track of "pathways" through various electronic manifolds. For many experiments, only a few pathways are important. Consider the first interaction with $\mathcal{V}$ in eq 2.7 and the subsequent time evolution in t_1. Initially, the density matrix is in the state $\rho(-\infty) = |g\rangle\rho_g\langle g|$. After the interaction with $\mathcal{V}$, the density matrix becomes a coherence:

$$\mathcal{V}\rho(-\infty) = |e\rangle[\mu_{eg}(\mathbf{Q})\rho_g]\langle g| - |g\rangle[\rho_g\mu_{ge}(\mathbf{Q})]\langle e| \quad (2.11a)$$

Since the electronic states are the eigenstates of the molecular Hamiltonian (eq 2.9), the time evolution of each term in this coherence involves only nuclear coordinates. For instance

$$\mathcal{G}(t_1)|g\rangle[\rho_g\mu_{ge}(\mathbf{Q})]\langle e| =$$
$$|g\rangle \exp(-iH_g t_1)[\rho_g\mu_{ge}(\mathbf{Q})] \exp(iH_e t_1)\langle e| \equiv$$
$$|g\rangle\mathcal{G}_{ge}(t_1)[\rho_g\mu_{ge}(\mathbf{Q})]\langle e| \quad (2.11b)$$

In general, we introduce the time evolution operator appropriate to a particular bra/ket electronic manifold as

$$\mathcal{G}_{\nu\nu'}(t)A \equiv \exp(-iH_\nu t)A \exp(iH_{\nu'}t) \qquad \nu, \nu' = g, f, e \quad (2.12)$$

where A is an arbitrary operator.

Since each $\mathcal{V}$ represents a commutator, which can act either from the left or from the right, $S^{(3)}$ will contain $2^3 = 8$ terms once these commutators are evaluated. These are the eight possible pathways representing the time ordering of the various interactions. These pathways come in complex conjugate pairs so that in
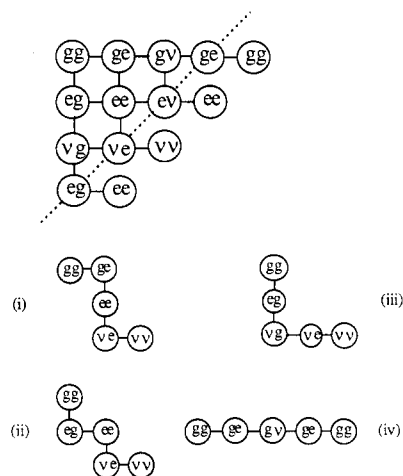

Figure 1. The Liouville space coupling scheme and the four pathways contributing to the nonlinear response function.[15] Initially, the electronic density matrix is $|g\rangle\langle g|$, which is denoted gg in the upper left corner. Solid lines denote the dipole interaction V. A horizontal (vertical) line represents an action of V from the right (left). Starting at the upper left corner there are $2^3 = 8$ third-order pathways in Liouville space, which lead to the dashed line and contribute to the third-order density matrix $\rho^{(3)}$. ν stands for either g or f (see eq 2.14). $P^{(3)}$ is calculated by acting on $\rho^{(3)}$ with V once more and taking a trace (eq 2.3). We note that the last V can act either from the left or from the right. The "right" choice in this figure is arbitrary. Out of the eight pathways, (i), (ii), (iii), and (iv) are shown in the figure, and they correspond respectively to R_1, R_2, R_3, and R_4 of eq 2.14. The other four pathways are the complex conjugates of these pathways.

practice we need to consider only four. In the following discussion, we invoke the Condon approximation and assume that the electronic transition dipole is independent of molecular nuclear degrees of freedom, i.e., $\mu_{eg}(\mathbf{Q}) = \mu_{eg}$ and $\mu_{fe}(\mathbf{Q}) = \mu_{fe}$. This approximation is not essential to the treatment that follows and can easily be relaxed (given that the transition dipole $\mu_{fe}(\mathbf{Q})$ is known). We thus get

$$S^{(3)}(t_3,t_2,t_1) = i \sum_{\alpha=1}^{4} [R_\alpha(t_3,t_2,t_1) - R_\alpha^*(t_3,t_2,t_1)] \quad (2.13)$$

The four independent pathways in the Condon approximation can be written in the form[15]

$$R_1(t_3,t_2,t_1) = \sum_{\nu=f,g} |\mu_{\nu e}|^2 |\mu_{eg}|^2 \, \mathrm{Tr} \, \{ \mathcal{G}_{\nu e}(t_3) \, \mathcal{G}_{ee}(t_2) \, \mathcal{G}_{ge}(t_1)\rho_g \}$$

$$R_2(t_3,t_2,t_1) = \sum_{\nu=f,g} |\mu_{\nu e}|^2 |\mu_{eg}|^2 \, \mathrm{Tr} \, \{ \mathcal{G}_{\nu e}(t_3) \, \mathcal{G}_{ee}(t_2) \, \mathcal{G}_{eg}(t_1)\rho_g \}$$

$$R_3(t_3,t_2,t_1) = \sum_{\nu=f,g} |\mu_{\nu e}|^2 |\mu_{eg}|^2 \, \mathrm{Tr} \, \{ \mathcal{G}_{\nu e}(t_3) \, \mathcal{G}_{\nu g}(t_2) \, \mathcal{G}_{eg}(t_1)\rho_g \}$$

$$R_4(t_3,t_2,t_1) = \sum_{\nu=f,g} |\mu_{\nu e}|^2 |\mu_{eg}|^2 \, \mathrm{Tr} \, \{ \mathcal{G}_{ge}(t_3) \, \mathcal{G}_{g\nu}(t_2) \, \mathcal{G}_{ge}(t_1)\rho_g \}$$

$$(2.14)$$

Here R_α^* is the complex conjugate of R_α. A pictorial representation of the four Liouville space pathways $R_1 \dots R_4$ is given in Figure 1.

III. The Probe Difference Absorption

The formal expressions presented in section II allow the calculation of a large variety of nonlinear spectroscopic observables. We now make a specific application to a model representing a pump–probe experiment[3,12] applied to a molecular system with three electronic levels. In a pump–probe experiment the system is subject to two light pulses. One is the pump pulse whose frequency is centered around ω_1. The other is the probe pulse whose frequency is centered around ω_2. The time delay of the probe pulse with respect to the pump pulse can be arbitrarily controlled. The probe absorption is then detected as a function of its frequency ω_2 and the time delay. To simplify the notation, we shall assume that the absorber is located at $r = 0$ and denote

$E(t) \equiv E(\mathbf{r},t)$ and $P(t) \equiv P(\mathbf{r},t)$. The external electric field in this experiment consists of two components:

$$E(t) = \hat{E}(\omega_1,t) + \hat{E}(\omega_2,t) \qquad (3.1a)$$

where

$$\hat{E}(\omega_1,t) = E(\omega_1,t) \exp(-i\omega_1 t) + E^*(\omega_1,t) \exp(i\omega_1 t) \qquad (3.1b)$$

$$\hat{E}(\omega_2,t) = E(\omega_2,t) \exp(-i\omega_2 t) + E^*(\omega_2,t) \exp(i\omega_2 t) \qquad (3.1c)$$

are the pump field and probe field with $E(\omega_1,t)$ and $E(\omega_2,t)$ being their temporal profiles, respectively. In a pump–probe experiment, provided both fields are sufficiently weak, we are interested in the third-order nonlinear polarization $P^{(3)}$ (eq 2.6), which may be expanded in the form

$$P^{(3)}(t) = \sum_s P^{(3)}(\omega_s,t) \exp(-i\omega_s t) \qquad (3.2)$$

The sum in eq 3.2 runs over all possible combinations of three frequencies: $\omega_s = \omega_j + \omega_k + \omega_l$ where $\omega_j, \omega_k, \omega_l = \pm\omega_1$ or $\pm\omega_2$. The probe absorption can be obtained by considering the total energy loss of the probe field and is related to the polarization of the medium by (Appendix A)

$$\sigma(\omega_2;\omega_1) = -\int_{-\infty}^{\infty} dt \; P(t) \frac{d}{dt} \hat{E}(\omega_2,t) \qquad (3.3)$$

where the probe field $\hat{E}(\omega_2,t)$ is given by eq 3.1c. The difference absorption $\Delta\sigma(\omega_2;\omega_1)$ is defined as the total probe absorption in the presence of pump pulse minus the probe absorption in the absence of the pump pulse. When eq 3.3 is evaluated, we obtain the difference absorption line shape (Appendix A)

$$\Delta\sigma(\omega_2;\omega_1) = 2\omega_2 \, \mathrm{Im} \int_{-\infty}^{\infty} dt \; E^*(\omega_2,t) \; P^{(3)}(\omega_2,t) \qquad (3.4)$$

where

$$P^{(3)}(\omega_2,t) = \sum_{j,k,l} \int_0^\infty dt_1 \int_0^\infty dt_2 \int_0^\infty dt_3$$

$$S^{(3)}(t_3,t_2,t_1) \exp[i(\omega_j + \omega_k + \omega_l)t_3 + i(\omega_j + \omega_k)t_2 + i\omega_j t_1] E(\omega_l,t-t_3) \; E(\omega_k,t-t_3-t_2) \; E(\omega_j,t-t_3-t_2-t_1) \qquad (3.5)$$

It is sometimes more convenient to disperse the probe pulse in frequency after its interaction with the system, rather than tune the probe. This detection is commonly used[3] and was considered by us earlier.[27] It is not identical with eq 3.4. $P^{(3)}(\omega_2,t)$ is the $\omega_s = \omega_2$ Fourier component of the third-order nonlinear polarization $P^{(3)}(t)$ (eq 3.2). The combination $\omega_2 = \omega_2 + \omega_2 - \omega_2$ does not contribute to the difference absorption signal, since it represents the saturated absorption of the probe in the absence of the pump field. The summation in eq 3.5 is over the $3! = 6$ permutations of $\omega_j, \omega_k, \omega_l$ with $\omega_1, -\omega_1$, and ω_2. For the molecular system with three electronic states (eq 2.9), $S^{(3)}$ has 16 terms (8 time orderings in eq 2.13 containing summations over two possible electronic states $\nu = g$ and f in eq 2.14. Therefore, there are altogether 6 × 16 = 96 terms when $P^{(3)}(\omega_2,t)$ (eq 3.5) is evaluated. Fortunately, only three of them survive (eq 3.8) if we make the following two approximations:

(1) The Rotating Wave Approximation (RWA). Some terms contain processes where a photon is absorbed and the system is excited (from g to e or from e to f) or conversely a photon is emitted and the system is deexcited. These processes are resonant and make a significant contribution to the signal. When at least one interaction violates this rule (e.g., a photon is absorbed and the system gets deexcited), this will result in a highly oscillatory off-resonant term which will make a negligible contribution. Within the rotating wave approximation we retain only resonant terms. This reduces the number of terms from 96 to 16.

(2) Optical Selectivity. In an ideal pump–probe experiment the frequency ω_{eg} of the $|g\rangle$ to $|e\rangle$ electronic transition is very different from the frequency ω_{fe} of the $|e\rangle$ to $|f\rangle$ electronic transition. The pump frequency ω_1 is tuned near resonance with ω_{eg}
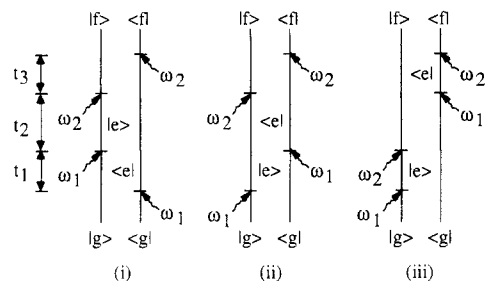

Figure 2. The three double-sided Feynman diagrams representing the probe difference absorption (eq 3.8) in the RWA and the optical selectivity approximation (eq 3.6). The Feynman diagrams may be obtained from the basic four pathways and their complex conjugates (Figure 1), using the rules given in Appendix B. Within the RWA an incoming arrow is accompanied by an increase in the system electronic quantum number (g to e, or e to f), whereas an outgoing arrow is accompanied by a decrease in the quantum number (f to e, or e to g). Optical selectivity implies that the pump ω_1 induces only a $|g\rangle$ to $|e\rangle$ transition while the probe ω_2 induces only an $|e\rangle$ to $|f\rangle$ transition. Time runs from the bottom to the top. The first, second, third, and fourth interactions take place at times $t - t_1 - t_2 - t_3$, $t - t_2 - t_3$, $t - t_3$ and t, respectively. t_1, t_2, and t_3 in eq 2.13 are therefore the intervals between successive interactions, as indicated in the figure. Diagrams i and ii result from pathways i and ii of Figure 1, respectively, and contribute to σ_I (eq 3.8b). Diagram iii comes from pathway iii of Figure 1 and contributes to σ_{II} (eq 3.8c).

while the probe frequency ω_2 is tuned near resonance with ω_{fe}. Consequently, we neglect all terms in which ω_1 induces an $|e\rangle$ to $|f\rangle$ transition or ω_2 induces an $|g\rangle$ to $|e\rangle$ transition. Approximations 1 and 2 amount to using the following simplified interaction with the electromagnetic field (cf. eq 2.2, 2.10, and 3.1):

$$H_{int} = -\mu_{eg}|e\rangle\langle g|E(\omega_1,t) \exp(-i\omega_1 t) - \mu_{fe}|f\rangle\langle e|E(\omega_2,t) \exp(-i\omega_2 t) + \mathrm{h.c.} \qquad (3.6)$$

where h.c. denotes the Hermitian conjugate. When both approximations are made, we are left with only three terms (rather than 96) which contribute to $P^{(3)}(\omega_2,t)$ (eq 3.5). Double-sided Feynman diagrams[13,28] provide a useful bookkeeping device for the various terms and interactions in the calculation of the molecular polarization. The representation of Figure 1 shows only the time ordering associated with each term. The Feynman diagrams show the complete terms (time ordering, choice of frequencies, and their sign). Appendix B gives the formal rules for using these diagrams. It suffices to say that each "side" of the diagram shows either the bra or the ket of the density matrix and that each arrow represents an interaction with the electromagnetic field. The three terms satisfying both the rotating wave approximation and optical selectivity are shown in Figure 2. Double-sided Feynman diagrams are a powerful tool for the analysis of nonlinear spectroscopies and, indeed, any process described by time-dependent perturbation theory of the Liouville equation. For instance, we see in Figure 2 that terms i and ii are in a *population* $|e\rangle\langle e|$ during the t_2 time period. Moreover, in these terms the pump always acts first and the probe acts second. This contrasts with term iii in Figure 2. Here, a population is *never* established on the excited-state surface $|e\rangle$. Also, this term has a mixed order of interaction between the pump and the probe. The separation of the observed signal into time-ordered (terms i and ii) and reverse-time-ordered (term iii) components is only possible in Liouville space. This separation is of direct physical significance. At short time delays between the pump and probe, term iii can dominate, leading to a spectrum that cannot be interpreted in terms of a "pump first, probe second" viewpoint.[14] If term iii is small, however, the effects of reverse time ordering can be neglected.

The generality of the double-sided Feynman diagrams also allows us to make analogies between apparently unrelated processes. For instance, terms i and ii are the exact analogues of fluorescence, with the proviso that the ω_2 photon must be emitted

(27) Loring, R. F.; Yan, Y. J.; Mukamel, S. *J. Chem. Phys.* **1987**, *87*, 5840; *J. Phys. Chem.* **1987**, *91*, 1302; *Chem. Phys. Lett.* **1987**, *135*, 23.

(28) Yee, T. K.; Gustafson, T. K. *Phys. Rev. A.* **1978**, *18*, 1597. Druet, S. A. J.; Taran, J. P. E. *Prog. Quantum Electron.* **1981**, *7*, 1.

rather than absorbed. Term iii, on the other hand, is directly analogous to Raman spectroscopy, where a population on the intermediate electronic surface is never established. Many other analogies can also be derived. For instance, term iii may represent the superexchange mechanism in electron transfer,[23b] where an electron proceeds from a state $|g\rangle$ through a high-energy intermediate state $|e\rangle$ to a final state $|f\rangle$. Since term iii never establishes a population on the intermediate-state surface, it can persist even when the intermediate state $|e\rangle$ is energetically forbidden. This property of term iii leads us to refer to it as a tunneling term.

Hereafter, we shall focus on ideal pump–probe experiments and consider only the three terms in Figure 2. We assume that the pump field is centered at $t = 0$ while the probe field is applied after the delay time $t = \tau$. To simplify the notation we define

$$E_1(t) \equiv E(\omega_1, t) \qquad (3.7a)$$

$$E_2(t-\tau) \equiv E(\omega_2, t) \qquad (3.7b)$$

as the temporal envelopes of the pump and probe fields, respectively. We further denote

$$\Delta\sigma(\omega_2, \tau; \omega_1) \equiv \Delta\sigma(\omega_2; \omega_1) \qquad (3.7c)$$

to specify explicitly the dependence of the absorption signal on the time delay, τ, between pump and probe pulses. By use of this notation (eq 3.7), the absorption signal (eq 3.4) can be written as

$$\Delta\sigma(\omega_2, \tau; \omega_1) = \omega_2 |\mu_{fe}|^2 |\mu_{eg}|^2 [\sigma_I + \sigma_{II}] \qquad (3.8a)$$

where

$$\sigma_I = 2 \operatorname{Re} \int_{-\infty}^{\infty} dt \int_0^{\infty} dt_3 \int_0^{\infty} dt_2 \int_0^{\infty} dt_1$$
$$\{\exp(i\omega_2 t_3 - i\omega_1 t_1) E_2^*(t+t_3-\tau)\ E_2(t-\tau)\ E_1(t-t_2)\ E_1^*(t-t_2-t_1)\ \times$$
$$\operatorname{Tr}\ [\mathcal{G}_{fe}(t_3)\ \mathcal{G}_{ee}(t_2)\ \mathcal{G}_{ge}(t_1)\rho_g] +$$
$$\exp(i\omega_2 t_3 + i\omega_1 t_1) E_2^*(t+t_3-\tau)\ E_2(t-\tau)\ E_1^*(t-t_2)\ E_1(t-t_2-t_1)\ \times$$
$$\operatorname{Tr}\ [\mathcal{G}_{fe}(t_3)\ \mathcal{G}_{ee}(t_2)\ \mathcal{G}_{eg}(t_1)\rho_g]\} \qquad (3.8b)$$

and

$$\sigma_{II} = 2 \operatorname{Re} \int_{-\infty}^{\infty} dt \int_0^{\infty} dt_3 \int_0^{\infty} dt_2 \int_0^{\infty} dt_1 \exp[i\omega_2 t_3 +$$
$$i(\omega_2 + \omega_1) t_2 + i\omega_1 t_1] E_2^*(t+t_3-\tau)\ E_1^*(t)\ E_2(t-t_2-\tau)\ \times$$
$$E_1(t-t_2-t_1)\ \operatorname{Tr}\ \{\mathcal{G}_{fe}(t_3)\ \mathcal{G}_{fg}(t_2)\ \mathcal{G}_{eg}(t_1)\rho_g\} \qquad (3.8c)$$

Equations 3.8a–3.8c are compact final formal expressions for the probe difference absorption signal. σ_I, which contains two terms, represented by (i) and (ii) of Figure 2, describes the processes in which the system interacts first with the pump and then with the probe fields. σ_{II}, which contains term iii of Figure 2, describes the processes in which one of the interactions with the probe field E_2 takes place between two interactions with the pump. In steady-state pump–probe experiments where the pump and the probe act simultaneously, all time orderings of the fields are equally important; this may give rise to interesting extra resonances.[14,29]

IV. Femtosecond Pump–Probe Spectroscopy: Entering through the Door and Observing through the Window

A pump–probe experiment is commonly viewed as consisting of three sequential steps: preparation, propagation, and detection. In subsection 1 we present a precise condition, called *ultrafast dephasing*, which allows pump–probe spectroscopy to be described in these terms. In the ultrafast dephasing limit, the probe absorption spectrum is given by the temporal convolution of the combined pump–probe intensity with a quantity that we call the bare spectrum. The bare spectrum represents a process consisting of instantaneous preparation, propagation for a definite time, and instantaneous detection. In subsection 2 we discuss a second limiting case of ultrashort pulses. If both the ultrafast dephasing limit and the ultrashort pulse limit hold, the bare spectrum is equal to the observed spectrum. Finally, in subsection 3 we consider the classical limit of our expressions. The classical Condon approximation is readily obtained as the classical limit of our theory.

1. Ultrafast Electronic Dephasing. The analysis is greatly simplified if we assume that the time scales t_1 and t_3 relevant in eq 3.8b are very short compared with the duration of the pulses E_1 and E_2. This assumption is easily justified in experiments involving very broad line shapes such as in condensed phases or in the ICN photodissociation. During the time periods t_1 and t_3 the system is in a *coherence*, and it is subject to fast *dephasing* processes which determine the line width of the corresponding spectral line. ($\mathcal{G}_{eg}(t_1)$ represents the $|g\rangle$ to $|e\rangle$ absorption process whereas $\mathcal{G}_{fe}(t_3)$ represents the $|e\rangle$ to $|f\rangle$ absorption process.) These dephasing processes also determine the relevant values of t_1 and t_3 which contribute to eq 3.8b. If dephasing processes are sufficiently rapid, we can neglect the variation of the external pulses on the t_1 and t_3 time scale, resulting in

$$E_1(t-t_2)\ E_1^*(t-t_2-t_1) \simeq |E_1(t-t_2)|^2 \equiv I_1(t-t_2) \qquad (4.1a)$$

$$E_2^*(t+t_3-\tau)\ E_2(t-\tau) \simeq |E_2(t-\tau)|^2 \equiv I_2(t-\tau) \qquad (4.1b)$$

We have defined here the temporal profiles of the pump and the probe pulses by $I_1(\tau)$ and $I_2(\tau)$, respectively. When eq 4.1 are substituted in eq 3.8b, we get

$$\sigma_I = \int_0^{\infty} dt_2\ I(\tau-t_2)\ \operatorname{Tr}\ \{\rho_W(\omega_2)\ \mathcal{G}_{ee}(t_2)\ \rho_D(\omega_1)\} \qquad (4.2)$$

where $I(\tau-t_2)$ is the convolution of intensities of the applied fields, i.e.

$$I(\tau-t_2) \equiv \int_{-\infty}^{\infty} dt\ I_2(t-\tau)\ I_1(t-t_2) \qquad (4.3)$$

In eq 4.2 we have defined the *doorway function*

$$\rho_D(\omega_1) = \int_0^{\infty} dt_1\ \exp(i\omega_1 t_1)[\exp(-iH_e t_1)\rho_g \exp(iH_g t_1)] + \text{h.c.}$$

$$\equiv \Phi_D(\omega_1) + \text{h.c.} \qquad (4.4)$$

and the *window function*

$$\rho_W(\omega_2) \equiv \int_0^{\infty} dt_3\ [\exp(iH_e t_3)\ \exp(-iH_f t_3)]\ \exp(i\omega_2 t_3) + \text{h.c.}$$

$$\equiv \Phi_W(\omega_2) + \text{h.c.} \qquad (4.5)$$

The associated doorway function amplitude $\Phi_D(\omega_1)$ and the window function amplitude $\Phi_W(\omega_2)$ are defined by eq 4.4 and 4.5, respectively. They will be used below in the definition of σ_{II}. h.c. denotes the Hermitian conjugate.

The significance of eq 4.2 is best illustrated if we use the Wigner representation. The Wigner function associated with an operator A is defined as

$$A(\mathbf{p}, \mathbf{q}) = \frac{1}{(2\pi\hbar)^N} \int_{-\infty}^{\infty} d\mathbf{s}\ \exp(-i\mathbf{p}\cdot\mathbf{s})\langle \mathbf{q} + \mathbf{s}/2|A|\mathbf{q} - \mathbf{s}/2\rangle \qquad (4.6)$$

The correlation function in eq 4.2 can then be written as

$$\operatorname{Tr}\ \{\rho_W(\omega_2)\ \mathcal{G}_{ee}(t_2)\ \rho_D(\omega_1)\} = \int d\mathbf{p}\ d\mathbf{q}\ \rho_W(\omega_2; \mathbf{p}, \mathbf{q})\ \rho_D(\omega_1; \mathbf{p}, \mathbf{q}, t_2) \qquad (4.7)$$

where $\rho_D(\omega_1; \mathbf{p}, \mathbf{q}, t_2)$ is the doorway function propagated for a time t_2 on the excited electronic surface $|e\rangle$.

Equation 4.7 thus offers the following simple physical picture: The doorway function $\rho_D(\omega_1; \mathbf{p}, \mathbf{q})$ is the Wigner function representing the state of the system prepared by the pump pulse with frequency ω_1. The doorway function then evolves in time for a period t_2, and its evolution is determined by the Hamiltonian H_e. At the end of that period we calculate the overlap of the resulting state with the window function $\rho_W(\omega_2; \mathbf{p}, \mathbf{q})$. ρ_W represents the region in phase space being observed when the probe frequency is ω_2. In short, the system enters the excited state through the door, propagates, and is then probed through the window.

The second term σ_{II} (eq 3.8c) does not offer a simple classical picture. During the t_2 period, it represents a coherent evolution of $|g\rangle$ and $|f\rangle$, very much analogous to Raman scattering or a two-photon absorption.[15b] The time ordering of the interactions

(29) Eichler, H. J.; Langhans, D.; Massmann, F. *Opt. Commun.* **1984**, *50*, 117. Balk, M. W.; Fleming, G. R. *J. Chem. Phys.* **1985**, *83*, 4300.

is pump, probe, pump, and we cannot interpret it as a probe of the state prepared by the pump. Furthermore, in σ_{II} all time arguments t_1, t_2, and t_3 represent the evolution of coherences and are all subject to fast electronic dephasing, which allows us to invoke a short time approximation:

$$E_1^*(t)\,E_1(t-t_2-t_1) \simeq |E_1(t)|^2 \equiv I_1(t) \qquad (4.8)$$

$$E_2^*(t+t_3-\tau)\,E_2(t-t_2-\tau) \simeq |E_2(t-\tau)|^2 \equiv I_2(t-\tau) \qquad (4.9)$$

When eq 4.8, 4.9, and 4.3 are substituted in eq 3.8c, we get

$$\sigma_{II} = 2I(\tau)\,\mathrm{Re}\,\int_0^\infty dt_2\,\exp[i(\omega_1+\omega_2)t_2]\,\times$$
$$\mathrm{Tr}\,\{\Phi_W(\omega_2)\,\mathscr{G}_{fg}(t_2)\,\Phi_D(\omega_1)\} \qquad (4.10)$$

We emphasize the fundamental difference between the doorway and the window *amplitudes* (Φ_D, Φ_W) which appear in σ_{II} and the doorway and the window *functions* (ρ_D, ρ_W) which appear in σ_I. The doorway amplitude prepares the system in an electronic coherence $|f\rangle\langle g|$ and $|g\rangle\langle f|$, and its evolution during the t_2 period is dominated by electronic dephasing arising from the difference in the Hamiltonians H_g and H_f. This evolution does not have a simple classical analogue. The doorway function prepares the system in the electronic state $|e\rangle\langle e|$, and its evolution during the t_2 period is the ordinary dynamics given by H_e, which has a well-defined classical analogue.

The correlation function in eq 4.10 can be written in the Wigner picture as

$$\mathrm{Tr}\,\{\Phi_W(\omega_2)\,\mathscr{G}_{fg}(t_2)\,\Phi_D(\omega_1)\} =$$
$$\int d\mathbf{p}\,d\mathbf{q}\,\Phi_W(\omega_2;\mathbf{p},\mathbf{q})\,\Phi_D(\omega_1;\mathbf{p},\mathbf{q},t_2) \qquad (4.11)$$

where the time evolution of the Wigner function is given by the coherent propagator from point $\mathbf{p}'\mathbf{q}'$ to point $\mathbf{pq}$ in phase space $\mathscr{G}_{fg}(\mathbf{p},\mathbf{q},\mathbf{p}',\mathbf{q}';t_2)$. Since the operators Φ_W and Φ_D are not Hermitian, the corresponding Wigner functions $\Phi_W(\mathbf{p},\mathbf{q})$ and $\Phi_D(\mathbf{p},\mathbf{q})$ are complex. The $I(\tau)$ factor in eq 4.10 implies that σ_{II} is nonzero only when the two pulses overlap. In an ideal pump–probe experiment, where the pulses are short and well-separated, σ_{II} vanishes. The time ordering associated with σ_{II} is responsible for extra holes in steady-state hole-burning experiments (where of course, we cannot control the relative time ordering of the two fields)[14] and for the "coherent artifact" in transient spectroscopy.[29]

2. Ultrashort Pulses. We consider here a second limiting case where the durations of the pulses are short compared to the time scale of molecular nuclear dynamics and to the delay time τ between them. In this case the contribution of σ_{II} (eq 3.8c) is negligible, and we need only consider σ_I (eq 3.8b). In the ultrashort pulse limit we can neglect the nuclear motion in the $|e\rangle$ state within the duration of the pulses. The absorption signal (eq 3.8a) may in this case be expressed in terms of a convolution with the power spectra of both pulses:

$$\sigma_I = \int_{-\infty}^\infty d\omega_2'\,\int_{-\infty}^\infty d\omega_1'\,\hat{I}_1(\omega_1-\omega_1')\,\hat{I}_2(\omega_2-\omega_2')\,\times$$
$$\mathrm{Tr}\,\{\rho_W(\omega_2')\,\mathscr{G}_{ee}(\tau)\,\rho_D(\omega_1')\} \qquad (4.12)$$

$$\sigma_{II} = 0 \qquad (4.13)$$

Here ρ_D and ρ_W are the doorway and window functions defined by eq 4.4 and 4.5, respectively, while $\hat{I}_1$ and $\hat{I}_2$ represent the power spectra of the pump and the probe fields, defined by

$$\hat{I}_j(\omega) = (2\pi)^{-1}\left|\int_{-\infty}^\infty dt\,\exp(-i\omega t)E_j(t)\right|^2;\quad j = 1, 2 \qquad (4.14)$$

The two limiting cases [of ultrafast dephasing and ultrashort pulses] discussed above simplify the way the external fields enter into the probe absorption. In both cases the fields enter into the final signal at their *intensity* level, and their phases are not important. These two limiting cases are not mutually exclusive. The ultrafast electronic dephasing limit holds when the pulses are long compared with the inverse line width of the corresponding optical transition. The ultrashort pulse limit holds when the pulses are short compared with their delay and the nuclear dynamics in the

excited state $|e\rangle$. If nuclear motion is much slower than the corresponding inverse line width, it is possible to adjust the duration of the pump and the probe pulses to be long compared to the electronic dephasing time but short compared to the time scale of nuclear motion so that both requirements are simultaneously met. In that case both limiting cases (eq 4.2 and 4.13) assume the common form

$$\sigma_I \propto \mathrm{Tr}\,\{\rho_W(\omega_2)\,\mathscr{G}_{ee}(\tau)\,\rho_D(\omega_1)\} \equiv \sigma_B(\omega_2,\tau;\omega_1) \qquad (4.15)$$

where we have denoted the spectrum in this case the "bare" spectrum σ_B. For pump–probe experiments in solution with extremely broad lines which are almost inhomogeneous, except for slow spectral diffusion processes, eq 4.15 provides an excellent description of the spectra.[27]

3. Classical Franck–Condon Approximation. We consider now the limiting case of classical nuclear dynamics. Recall that the relevant time scale of t_1 is the inverse line width of the $|g\rangle$ to $|e\rangle$ absorption profile. If this line width is broader than the vibronic frequency resolution, we can neglect the changes in the molecular momentum during the $|g\rangle$ to $|e\rangle$ transition. This is the classical Condon approximation. We also assume that the classical Condon approximation is valid for the $|e\rangle$ to $|f\rangle$ transition. In this case, H_g and H_e and H_e and H_f commute, and we can approximate the transition Green functions by

$$\mathscr{G}_{eg}(t_1) \sim \exp[-i(H_e - H_g)t_1] \equiv \exp(-iU_{eg}t_1) \qquad (4.16a)$$

$$\mathscr{G}_{fe}(t_3) \sim \exp[-i(H_f - H_e)t_3] \equiv \exp(-iU_{fe}t_3) \qquad (4.16b)$$

where

$$U_{eg} \equiv H_e - H_g = V_e - V_g \qquad (4.17a)$$

$$U_{fe} \equiv H_f - H_e = V_f - V_e \qquad (4.17b)$$

Using eq 4.16, the doorway function (eq 4.4) and the window function (eq 4.5) assume the form

$$\rho_D(\omega_1) = 2\pi\delta(\omega_1 - U_{eg})\rho_g \qquad (4.18a)$$

$$\rho_W(\omega_2) = 2\pi\delta(\omega_2 - U_{fe}) \qquad (4.18b)$$

In this case eq 4.7 or 4.15 reduces to

$$\mathrm{Tr}\,\{\rho_W(\omega_2)\,\mathscr{G}_{ee}(t_2)\,\rho_D(\omega_1)\} =$$
$$4\pi^2\,\mathrm{Tr}\,\{\delta(\omega_2 - U_{fe})\,\mathscr{G}_{ee}(t_2)\,\delta(\omega_1 - U_{eg})\rho_g\} \qquad (4.19)$$

Equation 4.19 corresponds to the classical Franck–Condon picture,[30] where the absorptions of ω_1 and ω_2 take place only at nuclear configurations where $U_{eg} = \omega_1$ and $U_{fe} = \omega_2$, respectively.

V. Femtosecond Photodissociation

The femtosecond photodissociation experiments of Rosker, Dantus, and Zewail[12] are outstanding examples of the ability of nonlinear spectroscopies to measure chemically relevant dynamical information—in this case the breaking of a chemical bond. Bersohn and Zewail[12c] have presented a classical theory of these experiments. In the classical picture, the probe difference absorption is given by eq 4.15 and 4.18 together, i.e.

$$\Delta\sigma(\omega_2,\tau;\omega_1) \propto \mathrm{Tr}\,\{\delta(\omega_2 - U_{fe})\,\mathscr{G}_{ee}(\tau)\,\delta(\omega_1 - U_{eg})\rho_g\} \qquad (5.1)$$

This is the extreme case in which we use all the three limiting cases in section IV simultaneously. In this picture the molecule interacts instantaneously with the pump field and moves into the excited electronic state $|e\rangle$. The evolution for the delay time τ on the excited-state $|e\rangle$ is further approximated by classical motion. Finally, the molecule again interacts instantaneously with the probe field, which raises the classical trajectory to the second excited state $|f\rangle$. During the delay time τ the molecule does not feel either the pump or the probe beam, so that the spectroscopy can be viewed as probing the free dynamics in the absence of the field. Our formal expression for the probe difference absorption is given by eq 3.8. The following approximations need to be made to recover eq 5.1: (i) The light pulses must be long compared to electronic dephasing processes (ultrafast electronic dephasing).
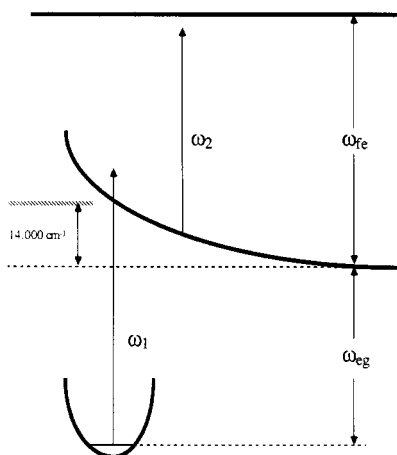
---

(30) Lax, M. *J. Chem. Phys.* **1952**, *20*, 1752.

Figure 3. The three potential energy surfaces of eq 5.2, and frequency definitions, are shown.

TABLE I: Parameters for the Hamiltonian of Eq 5.2

μ	21.59 amu	q_0	0.8 Å
ω_0	470 cm^{-1}	ω_{eg}	26100 cm^{-1}
V	14000 cm^{-1}	ω_{fe}	24600 cm^{-1}

(ii) The coherent pathway σ_{II} is neglected. This is justified in general if the light pulses are short compared to τ. (iii) The doorway function of eq 4.4, which represents the state prepared by the pump field, is replaced by its classical limit (eq 4.18a). Likewise, the window function of eq 4.5 is replaced by its classical limit (eq 4.18b). (iv) The quantum propagation during the delay time τ, given by $\mathcal{G}_{ee}(\tau)$, is replaced by a classical trajectory.

In this section we apply the doorway/window formalism to a simple model system, parametrized to roughly match the pump–probe photodissociation experiments on ICN carried out by Rosker, Dantus, and Zewail. We do not emphasize quantitative reproduction of the observed spectra. Rather, we focus on qualitative features and questions of interpretation. The model we pick has three electronic surfaces. The ground-state surface $|g\rangle$ is a harmonic oscillator, with parameters chosen to model the I–CN stretch in ICN. The first excited-state surface is a simple exponential repulsive wall, and the second excited-state surface is taken to be flat. Thus

$$H_g = \frac{p^2}{2\mu} + \frac{\mu\omega_0^2 q^2}{2} - \frac{1}{2}\hbar\omega_0$$

$$H_e = \frac{p^2}{2\mu} + V\exp(-q/q_0) + \hbar\omega_{eg}$$

$$H_f = \frac{p^2}{2\mu} + \hbar\omega_{eg} + \hbar\omega_{fe} \qquad (5.2)$$

$\hbar\omega_{eg}$ and $\hbar\omega_{fe}$ are the electronic energy differences between successive levels (see Figure 3). The parameters used in eq 5.1 are given in Table I. The parameters for H_g were obtained from the I–CN reduced mass (μ) and the I–CN stretch vibrational frequency given by Bersohn and Zewail.[12c] V is equal to the experimental maximum of the $|g\rangle$ to $|e\rangle$ absorption spectrum. q_0 was set to a value consistent with the time scale of femtosecond photodissociation observed by Rosker, Dantus, and Zewail.[12b]

The calculations in this section are made by using the doorway/window formalism in the limit of ultrafast electronic dephasing. This is valid, since the spectral line widths of the absorptions for $|g\rangle$ to $|e\rangle$ and $|e\rangle$ to $|f\rangle$ are on the order of 1000 cm^{-1}, which amounts to relevant time scales for t_1 and t_3 on the order of 5 fs: much shorter than the pulse durations ($\approx$100 fs) in this experiment. Furthermore, the observed time scale for molecular nuclear dynamics (i.e., bond breaking) is comparable to the duration of the pulses in use. This means that the ultrashort pulse limit is not valid in this experiment. We present detailed calculations of the doorway and the window functions as well as the
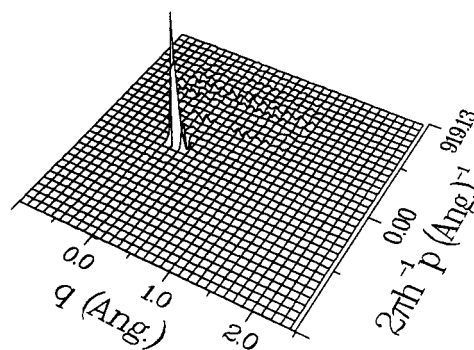

Figure 4. The doorway Wigner function $\rho_D(\omega_1;p,q)$ is shown for the Hamiltonian of eq 5.2 at zero temperature. The detuning from asymptotic resonance $\omega_1 - \omega_{eg} = 5000$ cm^{-1}.

probe absorption spectroscopy and explore the applicability of approximations i–iv implied in the classical picture of this spectroscopy. We start by considering the σ_I term and present fully quantum calculations of the doorway and the window functions. The extent to which the exact window and doorway functions differ from their delta function classical limit (eq 4.18) is a measure of the importance of quantum corrections in this experiment.

A. The Doorway Function. Let us first consider the doorway function for this problem which represents the state prepared by the pump laser (eq 4.4). In the molecular beam experiments we are considering, the system is thermally "cold" before interacting with the laser. Thus, we take the ground-state density matrix ρ_g to represent the ground state of H_g. A schematic of the energy levels and our frequency definitions is given in Figure 3. If one uses our parameters, the absorption line shape from $|g\rangle$ to $|e\rangle$ is a broad spectrum centered at $\omega_1 - \omega_{eg} = 14000$ cm^{-1} with fwhm of $\sim$1000 cm^{-1}.

We now turn to the practical calculation of the doorway function. Since we are dealing with a process at zero temperature, it is numerically advantageous to employ wave functions in the calculation of the doorway function. This does not in any way reduce the usefulness of the present Liouville space description. Our motivation for introducing a Liouville space treatment is primarily conceptual, as discussed in section I. For processes at finite temperatures, however, numerical procedures based directly on the density matrix are advantageous. For instance, one might imagine introducing a grid in phase space and then directly propagating the Wigner function on that grid, perhaps by a Fourier transform technique. Since the density matrix is assumed to be in the ground state of H_g, we find that

$$\langle x|\rho_D(\omega_1)|x'\rangle =$$

$$\langle x|\left[\int_0^\infty dt_1 \exp(i\omega_1 t_1) \exp(-iH_e t_1)|0_g\rangle\right]\langle 0_g|x'\rangle + \text{c.c.} \quad (5.3)$$

We employed the Fourier transform method developed by Feit and Fleck[31] to propagate the ground state of $H_g(|0_g\rangle)$ with the excited-state Hamiltonian H_e. The integral over t_1 was approximated by a Riemann sum, and the upper limit of the integral was replaced by a finite value t_{max}. To enhance the numerical convergence of the integral with respect to t_1, an exponential damping with time scale $t_{max}/5$ was used.

Although the (x,x') representation of the doorway function provides complete information, the Wigner representation is much more interpretable. We have calculated the Wigner function corresponding to ρ_D by means of the relation (cf. eq 4.6)

$$\rho_D(\omega_1;p,q) = \frac{1}{2\pi\hbar}\int_{-\infty}^{\infty} ds \exp(-ips)\langle q + s/2|\rho_D(\omega_1)|q - s/2\rangle \qquad (5.4)$$

The integral in eq 5.4 was evaluated with a standard fast Fourier transform routine. A plot of the doorway Wigner function when $\omega_1 - \omega_{eg} = 5000$ cm^{-1} is shown in Figure 4. (Recall that $\omega_1 -$

(31) Feit, M. D.; Fleck, Jr. J. A. *J. Chem. Phys.* **1983**, *78*, 301. Feit, M. D.; Fleck, Jr., J. A.; Steiger, A. *J. Comput. Phys.* **1982**, *47*, 412.
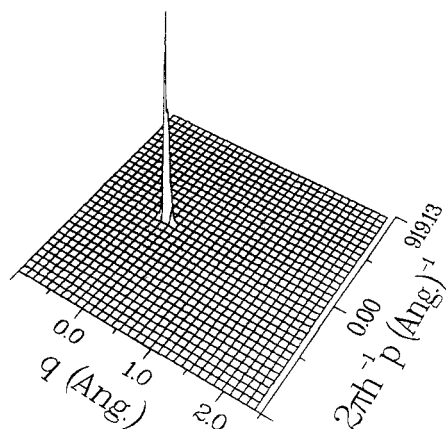
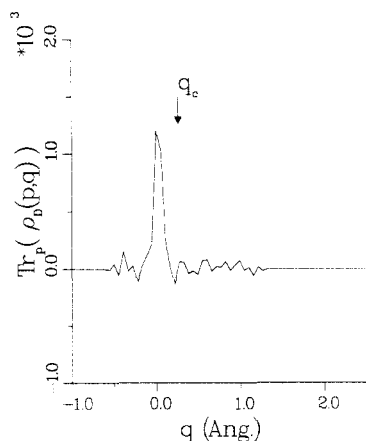**Figure 5.** The Wigner function of the ground state of H_g.

Figure 6. The trace over p of the doorway Wigner function of Figure 4 is shown. The trace shows localization in q similar to that of the ground-state Wigner function. Note that its maximum is shifted by ~ 0.3 Å from the classical Franck–Condon transition point q_c.

ω_{eg} is the detuning from the resonance between the bottom of the harmonic well and the *asymptote* of the $|e\rangle$ surface. The resonant value of the $|g\rangle \rightarrow |e\rangle$ transition corresponds to $\omega_1 - \omega_{eg} = 14\,000$ cm^{-1}.) The doorway Wigner function is localized in both momentum and position and is centered approximately around the origin. For the purpose of comparison, the Wigner function of the ground state $|0_g\rangle$ is plotted in Figure 5. The ground-state Wigner function and the doorway Wigner function are very similar. For all practical purposes, we can think of the doorway function as being the ground state of the $|g\rangle$ manifold lifted onto the $|e\rangle$ electronic manifold. This can be understood by the time–energy uncertainty principle. An absorption far off resonance occurs very quickly. Although it is electronically in $|e\rangle$ state, the doorway function does not have any time to distort from the initial nuclear configuration of the ground electronic state.

This picture, while not surprising, is in contradiction with the classical prediction. In the classical limit the doorway function becomes eq 4.18a—it is localized entirely at the point q_c at which the energy difference between the $|e\rangle$ and $|g\rangle$ potential energy surfaces is resonant with the pump energy. In Figure 6 the trace over p of the doorway shown in Figure 4 is given. Also shown in Figure 6 is q_c. The peak of the trace is noticeably shifted away by 0.3 Å from the classical prediction. The explanation for this behavior lies in the localization of ρ_g. We may view the off-resonant doorway function as resulting from a competition between a *classical* process occurring at the wings of the ground-state Wigner function and *tunneling* occurring at the maximum of the ground-state Wigner function. In this particular case tunneling appears to be the dominant contribution to the doorway function.

We next consider the doorway function when the pump field is resonant with the $|g\rangle$ to $|e\rangle$ absorption maximum. Figure 7 shows the doorway function obtained with a resonant pump laser $\omega_1 - \omega_{eg} = 14\,000$ cm^{-1}. The resonant function is delocalized over
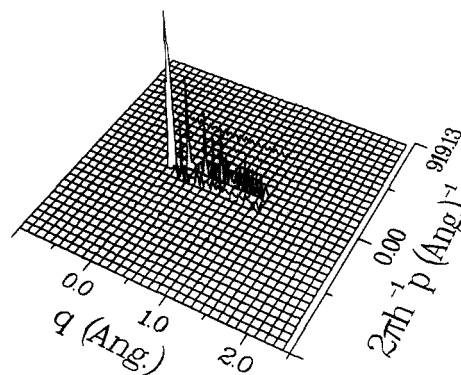

Figure 7. The doorway Wigner function is shown for $\omega_1 - \omega_{eg} = 14\,000$ cm^{-1}. The resonance doorway is spread over a much larger range of q values than the off-resonant doorway of Figure 4.
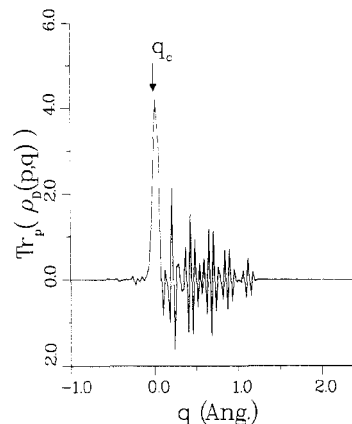

Figure 8. The trace over p of the doorway Wigner function of Figure 7 is shown. The trace is peaked near the classical value q_c, with oscillations occurring around the peak.

a much wider range of coordinate values than the off-resonant doorway of Figure 4. This is because the doorway state evolves in time for a much longer t_1 period (see eq 4.4) in the resonant case compared with the off-resonant case. The sharp peak in the doorway near $q = 0$ may be explained by a constructive interference near values of $q = 0$, that is, near the origin in coordinate. Figure 8 gives the trace over p of the resonant doorway. The trace is much more intense than the nonresonant trace shown in Figure 6, as might be expected. Also, the peak of the trace coincides almost exactly with the classical prediction. We can think of the resonant doorway as peaked about the classical value, but with very substantial width. This contrasts with the off-resonant doorway, which was not peaked about the classical value but had less width in coordinate. In both cases, the classical prediction does not give a complete qualitative picture of the quantum mechanical doorway function.

B. The Window Function. We next consider the window function (eq 4.5) and the associated Wigner representation of the window, defined in analogous way to eq 5.4. There is a close relation between the window function for a given pair of electronic states and the doorway for the same pair of electronic states. By inspection of eq 4.4 and 4.5, we see that a window function is proportional to a high-temperature doorway function for the same pair of states, i.e.

$$\rho_W(\omega) \sim \rho_D(-\omega) \quad \text{(high } T) \tag{5.5}$$

By the high-temperature argument it is reasonable to assume that a window function behaves more classically than a doorway, and that is precisely the result found below.

Before discussing the window functions further, however, we turn to the problem of their calculation. As a practical matter, window functions are harder to calculate than doorway functions. This is explained by the high-temperature analogy. The lack of any operator in the definition of the window function that is localized in phase space (such as ρ_g in the definition of the doorway
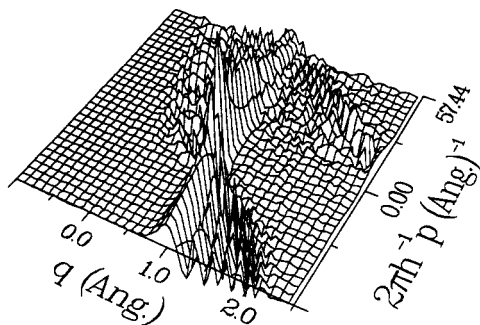
Figure 9. The window Wigner function with $\omega_2 - \omega_{fe} = -5000$ cm^{-1} is displayed. The window shows a ridge in q, surrounded by highly oscillatory regions.

function) means that the window function develops its localization through the cancellation of delocalized operators. In the classical limit (eq 4.18b), we expect a delta function in coordinate, a function that is localized in coordinate but uniform in momentum. The lack of localization of the operators in the definition of the window function makes grid methods based on direct Liouville space propagation of the density matrix difficult to implement. We have used an eigenstate-based method to calculate the window function. Namely, we introduce the expansions

$$\rho_W(\omega_2) \equiv \int_0^\infty dt_3 \ [\exp(iH_e t_3)\{\sum_\beta |\beta\rangle\langle\beta|\}\{\sum_\gamma |\gamma\rangle\langle\gamma|\} \times$$
$$\exp(-iH_f t_3)] \exp(i\omega_2 t_3) + \text{h.c.} \quad (5.6)$$

where $|\beta\rangle$ are the vibrational eigenstates of the $|e\rangle$ electronic manifold and $|\gamma\rangle$ are the vibrational eigenstates of the $|f\rangle$ electronic manifold. The coordinate representation of the window function is then

$$\langle x'|\rho_W(\omega_2)|x\rangle \equiv i\sum_{\beta,\gamma} \frac{\langle x'|\beta\rangle\langle\beta|\gamma\rangle\langle\gamma|x\rangle}{\omega_2 + \epsilon_\beta - \epsilon_\gamma + i\Gamma} + \text{c.c.} \quad (5.7)$$

Here ϵ_β and ϵ_γ are the eigenvalues corresponding to the vibrational eigenstates $|\beta\rangle$ and $|\gamma\rangle$ and Γ is the damping parameter that allows the integral in eq 5.6 to converge. In the calculations that follow, we take $\hbar/\Gamma = 60$ fs. Also, a slow exponential damping of the sums over β and γ was added to reduce finite basis set effects.

Equation 5.7 requires that a complete set of eigenfunctions and eigenvalues on both electronic manifolds, as well as the overlap between these eigenfunctions, be found. In practice, we calculate a finite but large number of eigenstates. We do this by enclosing the system in a box with infinite potential walls. At any given energy, the calculation of the wave function reduces to trajectory integration, with the position x playing the role of the time variable and the wave function $\psi(x)$ playing the role of one of the coordinates of the trajectory. To find the eigenstates, we do a Newton–Raphson search for energies such that the wave function vanishes at both ends of the box. The values of the wave functions are stored into an array, which reduces the evaluation of (5.7) to a sequence of matrix multiplications. Once the (x,x') matrix elements of ρ_W are found, we use fast Fourier transforms to find the Wigner function of ρ_W. The Wigner function thus obtained converges, for a fixed range of desired momentum values, as the number of eigenstates and the density of the (x,x') grid is increased.

Figure 9 gives a window function when $\omega_2 - \omega_{fe} = -5000$ cm^{-1} (shifted to the red 5000 cm^{-1} from the $|e\rangle \rightarrow |f\rangle$ asymptotic resonance), and Figure 10 gives a window function when $\omega_2 - \omega_{fe} = -2500$ cm^{-1}. Henceforth, we shall refer to the window in Figure 9 as window A, while the window in Figure 10 will be called window B. The window functions were produced by calculating 256 eigenfunctions on a grid of 2048 points. The results shown were checked for convergence by undertaking a smaller calculation involving 128 eigenstates on a 1024-point grid. The window functions obtained from the smaller calculation were in close agreement with those given here. The window functions show a localized "ridge" of positive values, surrounded by oscillatory
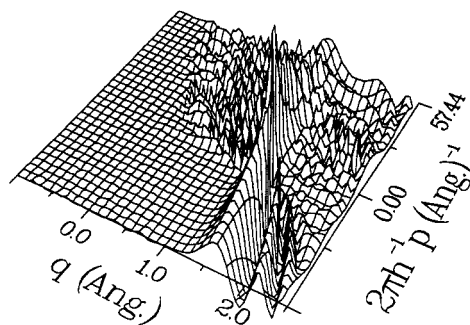

Figure 10. The window Wigner function with $\omega_2 - \omega_{fe} = -2500$ cm^{-1} is given. The ridge in the window is shifted to larger q values than that of Figure 9.
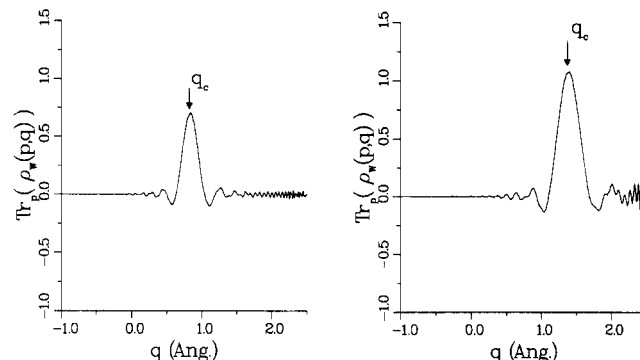

Figure 11. The trace over p of the window Wigner functions with $\omega_2 - \omega_{fe} = -5000$ cm^{-1} (left) and $\omega_2 - \omega_{fe} = -2500$ cm^{-1} (right) is displayed. The trace shows a clear shift as the frequency is changed. The peak of the window function corresponds closely to the classical prediction q_c.

regions. The "ridge" is located very close to the point predicted by the classical result (4.18b), which is 0.82 and 1.37 Å for window A and B, respectively. This is seen most clearly by considering the trace over p of the window function, which is displayed in Figure 11. The peak of the trace is seen to coincide almost exactly with the classical prediction for both values of the detuning. The peak in the trace for window B is higher and broader (in q) than that of window A.

The area under the peak has a simple classical interpretation. The classical window function is

$$\delta(\omega_2 - U_{fe}) = \frac{\delta(q - q_c)}{|U'_{fe}|_{q=q_c}} \quad (5.8)$$

Thus, the classical theory predicts that the area under the window function is proportional to the inverse of the slope of the potential difference, evaluated at the classical absorption point. The more parallel the potential surfaces involved, the greater the area. This prediction is in qualitative agreement with Figure 11, where the trace over p of window B is seen to have greater area than that of window A.

The width of the peak must be interpreted with caution. Although the peak of window B is more delocalized in coordinate than the peak of window A, that does not mean that the probe absorption spectrum is broader at the frequency associated with window B ($\omega_2 - \omega_{fe} = -2500$ cm^{-1}) than at the frequency associated with window A ($\omega_2 - \omega_{fe} = -5000$ cm^{-1}). To see this, we define the width in *energy* of the window function to be equal to

$$\Delta E \equiv |U_{fe}(q_1) - U_{fe}(q_2)| \quad (5.9)$$

where

$$\text{Tr}_p \ [\rho_W(p,q_1)] = \text{Tr}_p \ [\rho_W(p,q_2)] = \text{Tr}_p \ [\rho_W(p,q_c)]/2 \quad (5.10)$$

The energy width is a translation of the fwhm of the peak in the p trace of the window function into energy. Although the width in *coordinate* of window B is greater than that of window A, the width in *energy* is less. For instance, the ΔE of window A is 1700 cm^{-1}, whereas the ΔE of the peak of window B is 1100 cm^{-1}.
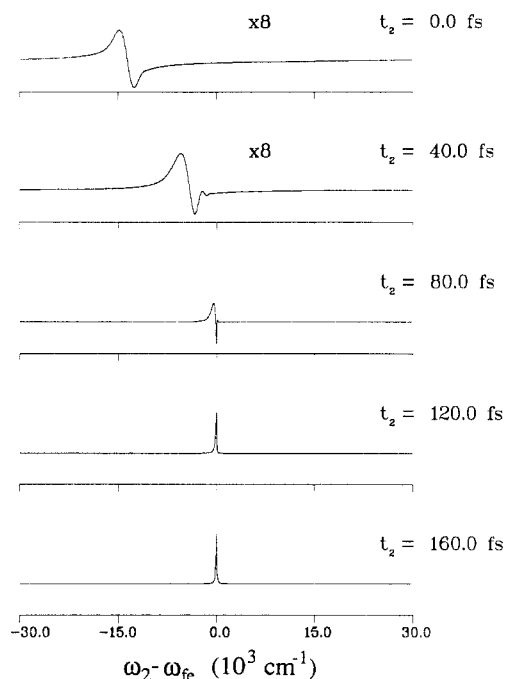
Figure 12. The bare spectrum $\sigma_B(\omega_2, t_2; \omega_1)$ (eq 4.15) is given with $\omega_1 - \omega_{eg} = 7100$ cm^{-1}, which is in the red wings of the pump absorption. The bare spectrum shows a clear increase in intensity as the delay time t_2 is increased. Furthermore, the spectrum shifts to the blue as t_2 increases, which is in agreement with the classical prediction.

C. Sequential Component of the Probe Absorption Spectrum. We now combine the doorway and the window functions to calculate the sequential part of the absorption σ_I (eq 4.2). Since the t_1 and t_3 time scales implied by the $|g\rangle \rightarrow |e\rangle$ and $|e\rangle \rightarrow |f\rangle$ absorptions are short compared to the E_1 and E_2 pulse duration, we are in the ultrafast electronic dephasing limit. This means that σ_I can be obtained by a temporal convolution of the bare spectrum (eq 4.15) and the pump–probe intensity profile. If the nuclear dynamics on the $|e\rangle$ surface were slow compared to the pulse delay, we would also be able to apply the ultrashort pulse limit, in which case σ_I would be given by the bare spectrum σ_B of eq 4.15. This is not the case in the present system; the temporal convolution is essential.

We have chosen to calculate the entire ω_2 spectrum at a fixed value of t_2. This is advantageous from a purely computational viewpoint, because it involves the propagation of operators that are localized in phase space and avoids the somewhat difficult calculation of the window function. To do this, we find the doorway function at fixed ω_1 and propagate it for a time t_2. We then do a propagation in t_3 instead of calculating a window function:

$$\sigma_B = 2 \; \text{Re} \int_0^\infty dt_3 \; \exp(i\omega_2 t_3 - \Gamma t_3) \; \text{Tr} \; [\mathcal{G}_{fe}(t_3) \; \mathcal{G}_{ee}(t_2) \; \rho_D(\omega_1)] \tag{5.11}$$

By storing the traces at incremental t_3 values, we can calculate the bare spectrum for all ω_2 at once. This must be repeated for each value of t_2 desired. In Figure 12 we give the resulting bare spectrum. The pump laser is at a frequency $\omega_1 - \omega_{eg} = 7100$ cm^{-1} (about 7000 cm^{-1} to the red of the absorption maximum). This reflects roughly the pump frequency used in the experiments of Rosker, Dantus, and Zewail.[12] The doorway function is localized at this frequency and is similar to the ground state. At $t_2 = 0$, the bare spectrum is very broad (about 8000 cm^{-1}) and shifted to the red. This reflects a rapid double vertical absorption from the ground state $|g\rangle$ through the first and second excited states $|e\rangle$ and $|f\rangle$. As t_2 is increased, the absorption narrows and gains intensity, until it reaches a stable asymptotic Lorentzian peak of width Γ. The bare spectrum never gains appreciable intensity to the blue of the asymptotic absorption maximum; any absorption to the blue occurs purely through tunneling. The shifting peak
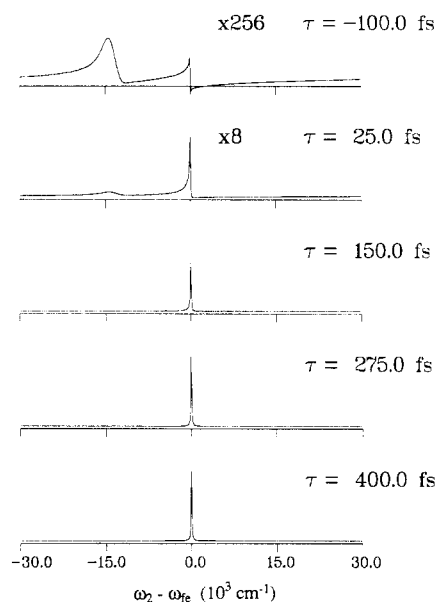

Figure 13. The observed spectrum for a Gaussian pump/probe intensity profile with a width of 200 fs and pump frequency $\omega_1 - \omega_{eg} = 7100$ cm^{-1} is shown. Note that the dynamics of Figure 12 is buried in the red wings of the observed spectrum.

of the bare spectrum is a clear indication of the underlying dissociative t_2 dynamics.

We next calculate the sequential spectrum σ_I associated with Figure 12. This is done by convoluting the bare spectrum (eq 5.11) with the pulse profile $I(t-\tau)$ as given by eq 4.2. We assume a Gaussian pump–probe intensity profile with a width of 100 fs. This is typical of the experiments of Zewail and co-workers (i.e., 50–150 fs). The 100-fs width, however, is long compared with the time it takes the bare spectrum to reach its asymptotic shape. This means that the observed spectrum, even at delay times of zero, is dominated by the intense asymptotic absorption maximum. The dissociation dynamics borne out so clearly in the bare spectrum of Figure 12 appears as activity in the wings of the observed spectrum. Figure 13 gives the observed spectrum. The peak of the spectrum starts out with a very small intensity for negative delay times and then increases until it reaches a constant asymptotic value. The activity in the red wings of the observed spectrum is largest compared with the peak for short or negaive delay times. The intensity in these areas starts at a small value, increases as the dynamics for times between 0 and 100 fs become more important, and then decreases. The behavior shown in Figure 13 was described by Zewail and co-workers but plotted as a function of delay time for fixed ω_1 and ω_2. In Figure 14 we give the spectrum plotted for varying τ, at fixed ω_2 and ω_1. For $\omega_2 \cong \omega_{fe}$, the spectrum rises and reaches an asymptotic value, while when ω_2 is tuned to the red of ω_{fe} the spectrum rises and then falls. It is important to remember that the rise and fall of the observed spectrum is not a direct observation of dynamics with $t_2 = \tau$, but rather of dynamics with different values of t_2 around τ convoluted with the pump–probe intensity profile (eq 4.2).

D. The Coherent (Tunneling) Term. In the preceding analysis, we considered only the σ_I term of the pump–probe spectrum, in which the pump acts first and then the probe acts second. When the laser fields have a substantial overlap in time, it is also possible for the coherent term σ_{II} to be important. In this term, the doorway *amplitude* is prepared by the pump and the probe coherently; so as for its window amplitude. A population on the $|e\rangle$ surface is never established in σ_{II}. We therefore refer to σ_{II} as a *tunneling* term. In the ultrafast dephasing limit the coherent term depends on the pump–probe delay time only through a constant of proportionality (eq 4.10). Thus, the coherent term contains *no direct dynamical information*; its dependence on the delay time τ simply reflects the profile of the incoming pulses.

We calculate the coherent term using the grid propagation technique of Feit and Fleck.[30] First, the doorway *amplitude*
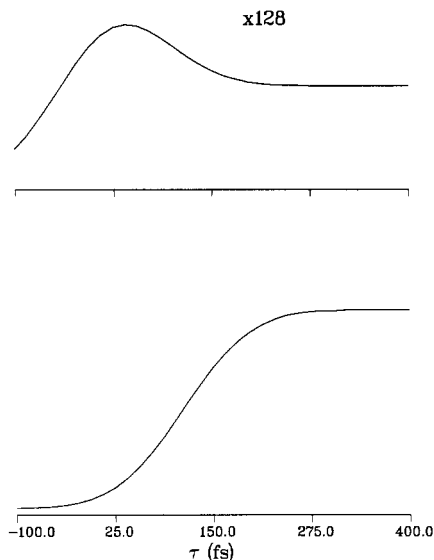
Figure 14. The observed spectrum is plotted versus delay time τ for two values of the probe frequency ω_2. The top plot gives the observed spectrum for $\omega_2 - \omega_{fe} = -16\,700$ cm^{-1}, while the bottom plot gives the observed spectrum for $\omega_2 - \omega_{fe} = 0$. The pump frequency $\omega_1 - \omega_{eg} = 7100$ cm^{-1}.

$\Phi_D(\omega_1)$ (not to be confused with the doorway *function* $\rho_D(\omega_1)$) is calculated at zero temperature by a wave function propagation and numerical integration:

$$\langle x|\Phi_D(\omega_1)|x'\rangle =$$
$$\langle x| \left\{ \int_0^\infty dt_1 \, \exp(-iH_e t_1 + i\omega_1 t_1 - \Gamma' t_1)|0_g\rangle \right\} \langle 0_g|x'\rangle \quad (5.12)$$

An exponential damping Γ' has been added to allow the integral in eq 4.13 to converge. The t_2 and t_3 evolutions can be similarly expressed entirely in terms of wave functions. Thus, direct Liouville space propagation is not required to find the coherent term at zero temperature.

Figure 15 gives the coherent term as a function of ω_2 for the pump frequency $\omega_1 = \omega_{eg} + 7100$ cm^{-1}. The function is oscillatory and shifted to the red of the asymptotic resonance. The red shift is a reflection of the short times involved throughout t_1, t_2, and t_3; the absorption takes place largely vertically. As the delay time τ increases, the shape of the coherent term does not change, while its intensity decreases due to the factor $I(\tau)$. In order to assess the significance of the coherent term, we need to check the relative intensity of σ_I and σ_{II}. If the intensity of the σ_{II} term is comparable to that of σ_I, the spectrum cannot be interpreted classically, since classical treatments (such as Bersohn and Zewail's) are based solely on the σ_I term. We have found that for our model system the peak of the coherent σ_{II} intensity is only about 10^{-3} times as intense as the peak of the σ_I spectrum at $\tau = 0$; reverse ordering of the pump and probe is therefore not significant in the particular experiment considered here, and σ_{II} can be neglected. It should be emphasized however that this conclusion is not universally true and σ_{II} does contribute significantly in other situations.[14] The role of σ_{II} in pump–probe spectroscopy should therefore always be carefully checked.

VI. Why Liouville Space?

At this point we address more fully the relationship between the Liouville space and wave function formulations of femtosecond pump–probe spectroscopy and point out at some length the advantages gained by a Liouville space picture. We first summarize the computationally simpler (at least for isolated molecules at zero temperature) way of calculating the pump–probe spectrum using the wave function and use this as a basis for analysis and comparison with the present picture. In this Hilbert space formalism the system is characterized by a wave function $\psi(t)$ which satisfies the time-dependent Schrödinger equation
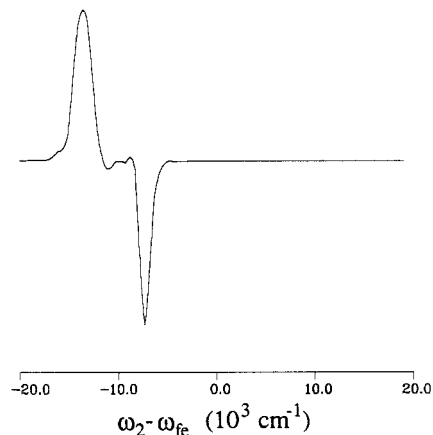
$$d\psi/dt = -iH_T(t)\psi \quad (6.1)$$

Figure 15. The coherent (tunneling) term is plotted versus ω_2 for a pump frequency $\omega_1 - \omega_{eg} = 7100$ cm^{-1}. The coherent term is much less intense (10^{-3}) than the incoherent term σ_I, even for zero pump/probe delay.

where H_T is given by eq 2.1. Let us assume that we are initially ($t = 0$) in an eigenstate of H_g, i.e., $|\psi(0)\rangle = |\alpha\rangle$. The amplitude of being in the vibronic state $|\gamma\rangle$ of the $|f\rangle$ manifold at time t is

$$C_{\gamma\alpha}(t) \equiv \langle\gamma|\psi(t)\rangle = \langle\gamma|\exp_+\left[-i\int_0^t d\tau \, H_T(\tau)\right]|\alpha\rangle \quad (6.2)$$

where $\exp_+$ is the time-ordered exponential. By use of eq 2.1 and 3.6, it is clear that the lowest order in H_{int} which contributes to $C_{\gamma\alpha}$ is second order. Up to a trivial phase factor we thus have

$$C_{\gamma\alpha}(t) = \int_0^t d\tau_1 \int_0^{\tau_1} d\tau_2 \, E_2(\tau_1) \, E_1(\tau_2) \, \exp(-i\omega_2\tau_1 - i\omega_1\tau_2) \times$$
$$\langle\gamma|\exp(iH_f\tau_1)V \exp[-iH_e(\tau_1 - \tau_2)]V \exp(-iH_g\tau_2)|\alpha\rangle$$

$$= \sum_\beta \mu_{\gamma\beta}\mu_{\beta\alpha} \int_0^t d\tau_1 \int_0^{\tau_1} d\tau_2 \, E_2(\tau_1) \, E_1(\tau_2) \times$$
$$\exp[-i(\omega_2 + \epsilon_\beta - \epsilon_\gamma)\tau_1 - i(\omega_1 + \epsilon_\alpha - \epsilon_\beta)\tau_2] \quad (6.3)$$

Here ϵ_α, ϵ_β, and ϵ_γ are the eigenvalues associated to $|\alpha\rangle$, $|\beta\rangle$, and $|\gamma\rangle$, the vibronic states of $|g\rangle$, $|e\rangle$, and $|f\rangle$ manifold, respectively. The probability of being in state $|\gamma\rangle$ at time t is $|C_{\gamma\alpha}(t)|^2$. Its time derivative is proportional to the cycle-averaged rate of absorption from the ω_2 field. If we integrate it over t, we get the total probe absorption. Finally, we need to average the result over the thermal distribution $P(\alpha)$ of initial states and sum over all the final states $|\gamma\rangle$. The probe absorption is then given by

$$\Delta\sigma(\omega_2,\tau,\omega_1) = \omega_2 \sum_{\alpha,\gamma} P(\alpha) \int_{-\infty}^\infty dt \, \frac{d}{dt}|C_{\gamma\alpha}(t)|^2 \quad (6.4)$$

Equation 6.4 together with eq 6.3 is identical with eq 3.8. In order to discuss the difference in appearance of these equations, let us first rearrange eq 6.4 by substituting eq 6.3 for $C_{\gamma\alpha}(t)$ and $C^*_{\gamma\alpha}(t)$. We can then carry out formally the sums over α and γ, resulting in[22a]

$$\Delta\sigma(\omega_2,\tau,\omega_1) = \omega_2 \int_{-\infty}^\infty dt \, \frac{d}{dt} \int_{-\infty}^t d\tau_1 \int_{-\infty}^{\tau_1} d\tau_2 \int_{-\infty}^t d\tau'_1 \int_{-\infty}^{\tau'_1} d\tau'_2$$
$$\langle\exp[iH_g(\tau'_2-\tau_2)]V \exp[iH_e(\tau'_1-\tau'_2)]V \exp[iH_f(\tau_1-\tau'_1)]V \times$$
$$\exp[-iH_e(\tau_1-\tau_2)]V\rho_g\rangle E_1(\tau_1) \, E_2(\tau_2) \, E^*_1(\tau'_1) \, E^*_2(\tau'_2) \times$$
$$\exp[-i\omega_2(\tau_1-\tau'_1) - i\omega_1(\tau_2-\tau'_2)] \quad (6.5)$$

Here τ_1 and τ_2 come from the expansion of the bra $C_{\gamma\alpha}(t)$ whereas τ'_1 and τ'_2 represent the ket $C^*_{\gamma\alpha}(t)$. Williams and Imre[32] have carried out a quantum mechanical calculation of the ICN pump–probe spectrum which was based on wave functions and Rayleigh-Schrödinger perturbation theory. Their calculation is equivalent to eq 6.5. Brown and Heller[33] have carried out a semiclassical calculation of the linear absorption spectrum of ICN, using the Wigner function. Their work is not in the spirit of the present treatment, however, since they use only diagonal $|e\rangle\langle e|$ propagation of the density matrix. This is only possible for a pure

(32) Williams, S. O.; Imre, D. G. *J. Phys. Chem.* **1988**, *92*, 6648.
(33) Brown, R. C.; Heller, E. J. *J. Chem. Phys.* **1981**, *75*, 186.

state in the absence of dephasing. Thus, that work is best regarded as the casting of pure state theory into a density matrix form, rather than a direct application of Liouville space ideas applicable to mixed states and condensed phases.

Let us now compare eq 3.8 with eq 6.5. Both equations are fourth order in the fields. Equation 3.8 has four time integrations; eq 6.5 has five integrations and one time derivative, which when performed reduces the number of integrations to four as well. The integration over t is common to both equations. We shall therefore consider only the other integrations. In the Liouville space form we integrate over t_1, t_2, and t_3 which are the *time intervals between successive interactions*. In the other form, τ_1 and τ_2 are the times of the interactions with the bra $C_{\gamma\alpha}(t)$ and τ'_1 and τ'_2 are the times of the two interactions with the ket $C^*_{\gamma\alpha}(t)$. τ_1 and τ_2 have a specific time ordering ($\tau_1 > \tau_2$) and so is τ'_1 and τ'_2 ($\tau'_1 > \tau'_2$). However, the relative time ordering of τ_1 and τ_2 with respect to τ'_1 and τ'_2 can be arbitrary, and we do not maintain the bookkeeping of their relative order in time. If we separate eq 6.5 into the various cases (e.g., whether τ_1 is before or after τ'_1, etc.), eq 6.5 will be separated into six terms corresponding respectively to the six terms of eq 3.8. In eq 6.5 the various time orderings of the ket and the bra interactions are lumped together, whereas in Liouville space each time ordering is calculated separately as a distinct Liouville space pathway (and Feynman diagram). It is straightforward to perform the change of variables in eq 6.5 and show its equivalence to eq 3.8.

In the following subsections, the advantages of a Liouville space description of condensed-phase spectroscopy are reviewed along with the advantages of a Liouville space description of ICN photodissociation. The orientation and overview below are particularly aimed at workers who specialize in gas-phase phenomena.

1. Thermal Averaging: Pure versus Mixed States. In Liouville space we calculate directly the signal using third-order perturbation theory. With the wave function we calculate a transition amplitude using second-order perturbation theory, and the signal is then related to the absolute square of that amplitude. The amplitude is calculated for a given pair of states, an initial state $|\alpha\rangle$ and a final state $|\gamma\rangle$. The result is then averaged over $|\alpha\rangle$ and summed over $|\gamma\rangle$. For small systems with a few degrees of freedom and at low temperatures, the summations over $|\alpha\rangle$ and $|\gamma\rangle$ do not cause a severe problem, and it may be easier to calculate an amplitude. The advantages of the Liouville space form are apparent for large systems at finite temperatures. In the Liouville space form we calculate directly the thermally averaged signal by propagating a density matrix representing a mixed state (rather than a pure state). No further averaging over thermal distributions is necessary.[15]

2. Physical Insight: Semiclassical Picture. Even in the case of a single degree of freedom at zero temperature, such as the molecular beam photodissociation of ICN, the Liouville space formulation provides better insight into the classical description of chemical dynamics. An equation analogous to eq 5.1 was proposed by Bersohn and Zewail[12c] to interpret the ICN experiment. Using the Liouville space formulation, we have shown how this expression may be obtained as a limit of σ_I. However, in addition we need to consider also the second term σ_{II}, which is important when the pump and the probe pulses are not well separated in time. This contribution does not have a simple classical analogue. In eq 6.5, obtained by using the wave function, both contributions $\sigma_I + \sigma_{II}$ are combined together, and the derivation of the classical result is much less transparent. There is a growing experimental and theoretical interest in studies of atomic and molecular clusters which interpolate between isolated molecules and condensed-phase systems.[34] One of the key questions is when is a system large enough to acquire bulk properties. By formulating the problem in Liouville space, we can treat small and large systems in a unified fashion and address these issues in a clear way.

3. Reduced Description: Role of Dephasing Processes. If we consider a molecular system in condensed phases (e.g., solution, polymer, or glass matrix, etc.), we must develop a *reduced description*[15] in which we follow explicitly only the dynamics of a few selected and relevant degrees of freedom. The remaining degrees of freedom are treated as a thermal bath by using statistical methods. The only practical way to obtain such a reduced description is by using the density matrix. This allows us to perform all the necessary averagings directly. When this is done, we find that the effects of the bath on the various terms σ_I and σ_{II} are profoundly different, which further demonstrates why we need to formulate the problem in Liouville space where these terms are naturally separated.

Consider an off-diagonal element of the density matrix such as ρ_{ge} or ρ_{ef}. When it evolves in time, it acquires a phase since its evolution from the left and the right is different. This phase depends on the state of the bath. When we consider an ensemble average of these elements over the distribution of the bath degrees of freedom, this phase results in a damping of these elements. This damping of off-diagonal elements of the density matrix resulting from phase (not amplitude) fluctuations is called *dephasing*. Dephasing processes can only be described in Liouville space, since in principle we can only distinguish between diagonal and off-diagonal elements of the density matrix in Liouville space. If we adopt a *complete description* with all degrees of freedom included, we do not need to introduce dephasing.[35] However, this is impractical for realistic condensed-phase systems. A beautiful analogy is the concept of entropy in thermodynamics. In a complete dynamical description of a system we do not need to invoke this concept; however, on the greatly reduced thermodynamic level, entropy is essential for a proper description of the system.

4. Interference among Liouville Space Pathways: Dephasing-Induced Phenomena. Since the various Liouville space pathways are complex quantities, thay may interfere when added. This interference has in many cases a dramatic effect on experimental observables. Dephasing processes in linear optics simply cause line broadening.[13,15] In nonlinear optics dephasing processes can affect the interference among Liouville space pathways and induce new spectral features. To be specific, let us consider first the result of a stationary pump–probe experiment. To that end we assume that the field amplitudes $E_1(t)$ and $E_2(t)$ are time independent and set $E_1(t) = E_2(t) = 1$. The stationary signal $\Delta\sigma_s(\omega_2,\omega_1)$ is then defined by eq 6.4 or 3.8 by simply eliminating the integration over t since in a steady-state experiment we measure the rate of photon absorption rather than the integrated absorption. Then eq 6.4 reduces to the familiar Kramers–Heisenberg form:[15]

$$\Delta\sigma_s(\omega_2,\omega_1) = 2\pi\sum_{\alpha,\gamma}P(\alpha)\left|\sum_\beta \frac{\mu_{\gamma\beta}\mu_{\beta\alpha}}{\epsilon_\alpha - \epsilon_\beta + \omega_1}\right|^2 \delta(\epsilon_\alpha - \epsilon_\gamma + \omega_1 + \omega_2)$$

(6.6)

In our Liouville space description of the steady-state experiment σ_{II} is separated into two terms. One term is exactly equal to $-\sigma_I$ and cancels it. This is a dramatic example of destructive interference. The remaining portion of σ_{II} results in eq 6.6. A discussion of this interference was made recently for the analogous problem of Raman and fluorescence spectra.[15b] When we calculate the spectrum of light emitted from a system excited by a stationary pump at ω_1, we find the same pathways considered here. σ_I and part of σ_{II} contribute to a fluorescence spectrum which is broad, and the other part of σ_{II} gives rise to the Raman spectrum which is written in the Kramers–Heisenberg form (eq 6.6). In the absence of a thermal bath and dephasing processes, the fluorescence exactly cancels due to the interference between σ_I and σ_{II} and the entire spectrum is of the Raman type. When dephasing processes are introduced, the exact cancellation which occurs in the absence of dephasing no longer holds, and the spectrum is separated in a sharp (Raman) and a broad bath induced fluorescence.

(34) Hahn, M. Y.; Whetten, R. L. *Phys. Rev. Lett.* **1988**, *61*, 1190.

(35) Mukamel, S. *Chem. Phys.* **1978**, *31*, 327. Shan, K.; Yan, Y. J.; Mukamel, S. *J. Chem. Phys.* **1987**, *87*, 2021.

Another dramatic example of the role of dephasing occurs in four-wave mixing.[15b,c,36] Four-wave mixing is a $\chi^{(3)}$ process described by the same response function $S^{(3)}$ (eq 2.7) introduced here. Consider a four-wave mixing experiment in which two stationary light beams with frequencies ω_1 and ω_2 and wavevectors k_1 and k_2 interact and produce a signal with $k_s = 2k_1 - k_2$ and $\omega_s = 2\omega_1 - \omega_2$. As ω_1 is scanned versus ω_2, it is found that a resonance can occur whenever $\omega_1 - \omega_2$ is equal to an energy difference between two ground-state vibrational levels. This resonance is called CARS (coherent anti-Stokes Raman) and is the coherent analogue of spontaneous Raman.[36] In addition, it was found that as the pressure of a foreign gas is increased[37] or as the temperature is raised in a molecular crystal,[38] new sharp resonances appear when $\omega_1 - \omega_2$ is equal to a difference of energy between excited-state levels. The surprising aspect of these resonances is that we usually expect the dephasing rate to increase at high pressures or high temperatures. This should broaden the spectral lines and destroy sharp features of the spectrum (e.g., the transition from Raman to fluorescence). In this case the opposite happens; dephasing destroys the exact cancellation of Liouville space pathways, which results in the appearance of new sharp lines. These examples show how crucial the role of dephasing (which can only be described in Liouville space) is in nonlinear spectroscopy.

VII. Conclusion

In this paper, we present a theory of femtosecond pump–probe photodissociation that is based on the density matrix and techniques of nonlinear optics. Although a theoretical treatment based on wave functions would have been simpler to derive and implement numerically, we are convinced that the present treatment has yielded dividends that are more than adequate. Using Liouville space, we have been able to cast the exact expression for the probe absorption spectrum in the limit of ultrafast dephasing into a form (eq 4.2) that is closely related to the classical Condon approximation. This form involves the temporal convolution of a new quantity, which we call the *bare spectrum*, with the combined pump–probe intensity profile. The bare spectrum has a physically appealing form: it corresponds to a process where the pump instantaneously prepares a state, which then propagates in the absence of the field for a definite time, and is finally probed instantaneously by the probe laser. We call the state prepared by the pump laser a *doorway function*. The probing action of the second laser is represented by a *window function*. We also identify a second simplifying case, called the ultrashort pulse limit, where the observed signal is given by a spectral convolution of the bare spectrum with the spectral intensity profile of the laser pulses.

We apply these new interpretive concepts to the photodissociation of ICN. We find that the femtosecond pump–probe experiments of Rosker, Dantus, and Zewail on ICN is in the ultrafast dephasing limit, because of the large spectral widths of the pump and probe absorptions, but is not in the ultrashort pulse limit. This means that the bare spectrum is substantially different from the observed spectrum. This does not mean, however, that the concept of the bare spectrum is without validity in the photodissociation of ICN. We find that the bare spectrum shows the ICN dissociative dynamics much more clearly than the observed spectrum. The shift of the probe absorption to the blue as the time delay is increased is seen as activity in the *wings* of the observed spectrum but is seen as shifting of the *peak* of the bare spectrum. The bare spectrum may be obtained by deconvoluting the observed spectrum with the pump–probe intensity profile. Also, the bare spectrum corresponds to a process with a *definite* time of propagation. We believe that the bare spectrum may become a useful concept in understanding femtosecond pump–

probe experiments, especially those in which the underlying dynamics is more complicated than the simple dissociation of the ICN model presented here.

We also examine the doorway and window functions for model ICN in some detail. This represents a pictorial analysis of the importance of quantum corrections in ICN pump–probe photodissociation. We find that the peak (as a function of dissociation coordinate) of the window function closely follows the prediction of the classical Condon approximation but that these functions have substantial width and complicated oscillations. This points to the importance of quantum corrections in developing a quantitative theory of the ICN experiments but validates the qualitative conclusions of classical models. Doorway functions, on the other hand, are found to have peaks that differ from the classical prediction. We interpret this in terms of an interesting competition betwen tunneling at the maximum of the ground-state wave function and a classically allowed process at the wings of the ground-state wave function.

We have put Liouville space formalism to work in understanding zero-temperature, gas-phase femtosecond photodissociation. One of the advantages our approach, however, is that we are necessarily limited to such systems. Benjamin and Wilson[39] have recently published a quasiclassical computer simulation of ICN femtosecond pump–probe dissociation in the liquid phase. Femtosecond photodissociation experiments in the condensed phase will surely appear in a short period of time. The ideas presented here are applicable to such problems. In our opinion, much more work is needed on the development of ideas, methodologies, and algorithms that can make the transition between the seemingly disparate worlds of gas-phase and condensed-phase phenomena.

Appendix A. The Probe Absorption Spectrum: Derivation of Eq 3.3 and 3.4

We start our derivation by considering the mean energy loss of the probe when it passes through the optical medium. The mean energy loss at time t is given by

$$\frac{\partial}{\partial t} \langle H_{\text{int}}(\omega_2, t) \rangle = \text{Tr}\left[\frac{\partial}{\partial t} H_{\text{int}}(\omega_2, t)\, \rho(t)\right] \quad \text{(A.1)}$$

Here $\rho(t)$ is the density matrix of the system defined by eq 2.4 and $H_{\text{int}}(\omega_2, t)$ represents the interaction between the optical medium and the probe field $\hat{E}(\omega_2, t)$ (eq 3.1c). We have

$$H_{\text{int}}(\omega_2, t) = -V\hat{E}(\omega_2, t) \quad \text{(A.2)}$$

When eq A.2 is substituted in eq A.1 and followed by using eq 2.3, we obtain

$$\frac{\partial}{\partial t} \langle H_{\text{int}}(\omega_2, t) \rangle = -P(t)\frac{\partial}{\partial t}\hat{E}(\omega_2, t) \quad \text{(A.3)}$$

The absorption signal at ω_2 is obtained by taking the average of eq A.3 over an optical cycle and following the integration over t. This results in eq 3.3.

We expand the total external field as follows (cf. eq 3.1):

$$E(t) = \sum_j E(\omega_j, t)\, \exp(-i\omega_j t) + \text{c.c.} \quad \text{(A.4)}$$

In this case, the molecular polarization has the form

$$P(t) = \sum_s P(\omega_s, t)\, \exp(-i\omega_s t) + \text{c.c.} \quad \text{(A.5)}$$

The frequency $\omega_s \geq 0$ in eq A.5 can be any combination of the field frequencies $\{\pm\omega_j\}$. In the slowly varying amplitude approximation where we assume that the temporal envelope of the

(36) Bloembergen, N.; Lotem, H.; Lynch, R. T. *Indian J. Pure Appl. Phys.* **1978**, *16*, 151.
(37) Rothberg, L. J.; Bloembergen, N. *Phys. Rev. A* **1984**, *30*, 820.
(38) Andrews, J. R.; Hochstrasser, R. M. *Chem. Phys. Lett.* **1981**, *82*, 381. Andrews, J. R.; Hochstrasser, R. M.; Tromsdorff, H. P. *Chem. Phys.* **1981**, *62*, 87.

(39) Benjamin, I.; Wilson, K. R. *J. Chem. Phys.* **1989**, *90*, 4176.

probe field (eq 3.1c) varies slowly in time compared to its optical frequency, i.e.

$$\frac{\partial}{\partial t}E(\omega_2,t) \ll \omega_2 E(\omega_2,t) \qquad (A.6)$$

In this case

$$\frac{\partial}{\partial t}\hat{E}(\omega_2,t) \approx -i\omega_2[E(\omega_2,t)\ \exp(-i\omega_2 t) - E^*(\omega_2,t)\ \exp(i\omega_2 t)]$$
$$(A.7)$$

Substituting eq A.5 and A.7 into eq A.3, we obtain

$$\frac{\partial}{\partial t}\langle H_{int}(\omega_2,t)\rangle = \omega_2 \sum_s \{iE^*(\omega_2,t)\ P(\omega_s,t)\ \exp[i(\omega_2 - \omega_s)t] - iE(\omega_2,t)\ P(\omega_s,t)\ \exp[-i(\omega_2 + \omega_s)t]\} + c.c. \quad (A.8)$$

The only contribution from eq A.8 after the averaging over an optical cycle is the term with $\omega_s = \omega_2$. We finally obtain

$$\sigma(\omega_2) = 2\omega_2\ \text{Im}\ \int_{-\infty}^{\infty}dt\ E^*(\omega_2,t)\ P(\omega_2,t) \qquad (A.9)$$

which proves eq 3.4.

Appendix B. Rules for Double-Sided Feynman Diagrams

Double-sided Feynman diagrams can be introduced by the following set of rules,[28] which relate the diagrams to terms in the perturbation expansion of the Liouville operator.

(i) The density matrix is represented by two vertical lines. The line on the left represents the ket, and the line on the right represents the bra.

(ii) The time runs vertically from bottom to top.

(iii) An interaction with the radiation field is represented by a wavy line.

(iv) Each diagram has an overall sign of $(-1)^n$ where n is the number of interactions from the right (bra). This is because each time a V acts from the right in a commutator it has a minus sign.

(v) Each interaction is assigned to an arrow and labeled by the corresponding field ω_j (>0). Incoming arrows represent photon absorption while outgoing arrows represent photon emission.

(vi) An incoming arrow on the left or an outgoing arrow on the right represents a photon annihilation (ω_j) and will contribute a factor $E(\omega_j,t)\ \exp(-i\omega_j t)$ to the diagram. Conversely, an outgoing arrow on the left or an incoming arrow on the right represents a photon creation ($-\omega_j$) and contributes a factor $E^*(\omega_j,t)\ \exp(i\omega_j t)$ to the diagram. The overall frequency of the term is the sum of the three interactions ω_j, ω_k, and ω_l with their appropriate signs.

In the Feynman diagrams of Figure 2 we include also the fourth interaction at time t with $E^*(\omega_2,t)$ by an incoming arrow on the right. This represents probing the final absorption signal (eq 3.4).

Temperature Dependence of the Electronic-to-Vibrational Quenching Rate Constants of NF(b$^1\Sigma^+$)

X. Y. Bao and D. W. Setser*

Department of Chemistry, Kansas State University, Manhattan, Kansas 66506 (Received: December 22, 1988; In Final Form: June 9, 1989)

The temperature dependence of the quenching rate constants of NF(b) by 18 different reagents has been measured in a flow reactor over the 530–200 K range. The rate constants for O_2, H_2, D_2, HCl, CO_2, and CO were fitted to an Arrhenius dependence on temperature, but the rate constants for the other molecules generally have a weaker dependence on temperature. The temperature dependence of the rate constant and the hydrogen–deuterium isotope effect for several pairs of molecules are discussed in terms of the expected exit channels for quenching by electronic-to-vibrational energy transfer.

I. Introduction

There has been continued interest in the chemistry of NF-(a$^1\Delta$;11 435 cm^{-1}) and NF(b$^1\Sigma^+$;18 905 cm^{-1}) because of their potential for utilization as chemical energy storage sources.[1-3] In particular, the NF(b) state has been considered as a candidate for excitation-transfer laser systems.[4,5] The NF(a) state can be efficiently produced by two reactions, H + NF$_2$ and F + N$_3$.[3,6] Subsequent formation of NF(b) can be achieved by energy-pooling reactions from I($^2P_{1/2}$), HF(v=2), or O_2(a$^1\Delta$).[4,7-9] In addition

to these practical considerations, the NF(a) and NF(b) states offer the opportunity to study reactions of electronically excited singlet molecules. A general understanding of electronic-to-vibrational (E–V) energy transfer is particularly lacking, and the NF(a and b) states can be systematically studied and compared with the isoelectronic O_2 states (a$^1\Delta_g$;7918 cm^{-1} and b$^1\Sigma_g^+$;13 195 cm^{-1}) to generate a data base.

Our laboratory has utilized a NF(b) source based upon the metastable Ar flowing afterglow technique.[5,10] Quenching rate constants for halogens and inter-halogens[5] and a comprehensive study of quenching by diatomic and small polyatomic molecules at 300 K have been reported.[10] Except for the halogens, there was no evidence for quenching by chemical reaction and the quenching mechanism was assigned as E–V transfer with formation of NF(a). In this paper, we have extended the quenching measurements to both higher ($\leq$530 K) and lower (200 K) temperature for diatomic, triatomic, and small polyatomic molecules. The deuterium isotope effect on the quenching rate constants also was studied for the following pairs of molecules: H_2 vs D_2, H_2O vs D_2O, CH_3OH vs CH_3OD, $(CH_3)_2CO$ vs $(CD_3)_2CO$, and CH_2Cl_2 vs CD_2Cl_2. The temperature dependence of the rate

(1) (a) Clyne, M. A. A.; White, I. F. *Chem. Phys. Lett.* **1970**, *26*, 465. (b) Cheah, C. T.; Clyne, M. A. A. *J. Photochem.* **1981**, *15*, 21.

(2) Herbelin, J. M.; Cohen, N. *Chem. Phys. Lett.* **1973**, *20*, 605.

(3) Malins, R. J.; Setser, D. W. *J. Phys. Chem.* **1981**, *85*, 1342.

(4) (a) Pritt, A. T., Jr.; Patel, D.; Benard, D. J. *Chem. Phys. Lett.* **1983**, *97*, 471. (b) Pritt, A. T., Jr.; Benard, D. J. *J. Phys. Chem.* **1986**, *85*, 7159.

(5) Cha, H.; Setser, D. W. *J. Phys. Chem.* **1987**, *91*, 3758.

(6) (a) Coombe, R. D.; Pritt, A. T., Jr. *Chem. Phys. Lett.* **1978**, *58*, 606. (b) Habdas, J.; Wategaonkar, S.; Setser, D. W. *J. Phys. Chem.* **1987**, *91*, 451.

(7) Herbelin, J. M.; Kwok, M. A.; Spencer, D. J. *J. Appl. Phys.* **1978**, *49*, 3750. The observations given here must be adjusted for the currently accepted NF(a) lifetime.

(8) Habdas, J.; Setser, D. W. *J. Phys. Chem.* **1989**, *93*, 229.

(9) (a) Hack, A.; Horie, O. *Chem. Phys. Lett.* **1981**, *82*, 327. (b) Patel, D.; Pritt, A. T.; Benard, D. J. *Chem. Phys. Lett.* **1984**, *107*, 105.

(10) Cha, H.; Setser, D. W. *J. Phys. Chem.* **1988**, *93*, 235.